Wireless Infrared Communications

JOSEPH M. KAHN, MEMBER, IEEE, AND JOHN R. BARRY

The use of infrared radiation as a medium for high-speed, short-range wireless digital communication is discussed. Currently available infrared links and local-area networks are described. Advantages and drawbacks of the infrared medium are compared to those of radio and microwave media. Physical characteristics of infrared channels using intensity modulation with direct detection (IM/DD) are presented, including path losses and multipath responses. Natural and artificial ambient infrared noise sources are characterized. Strategies for designs of transmitters and receivers that maximize link signal-to-noise ratio (SNR) are described. Several modulation formats are discussed in detail, including on–off keying (OOK), pulse-position modulation (PPM), and subcarrier modulation. The performance of these techniques in the presence of multipath distortion is quantified. Techniques for multiplexing the transmissions of different users are reviewed. Performance of an experimental 50-Mb/s on–off-keyed diffuse infrared link is described.

I. INTRODUCTION

The emergence of portable information terminals in work and living environments is accelerating the introduction of wireless digital links and local area networks (LAN's). Portable terminals should have access to all of the services that are available on high-speed wired networks. Unlike their wired counterparts, portable devices are subject to severe limitations on power consumption, size and weight. The desire for inexpensive, high-speed links satisfying these requirements has motivated recent interest in infrared wireless communication [1]–[44].

A. Comparison Between Infrared and Radio Media

As a medium for short-range, indoor communication, infrared[1] radiation offers several significant advantages over radio.[2] Infrared emitters and detectors capable of high-speed operation are available at low cost. The infrared spectral region offers a virtually unlimited bandwidth that is unregulated worldwide. Infrared and visible light are close together in wavelength, and they exhibit qualitatively similar behavior. Both are absorbed by dark objects, diffusely reflected by light-colored objects, and directionally reflected from shiny surfaces. Both types of light penetrate through glass, but not through walls or other opaque barriers, so that infrared transmissions are confined to the room in which they originate. This signal confinement makes it easy to secure transmissions against casual eavesdropping, and it prevents interference between links operating in different rooms. Thus, infrared wireless LAN's can potentially achieve a very high aggregate capacity, and their design may be simplified, since transmissions in different rooms need not be coordinated. When an infrared link employs intensity modulation with direct detection (IM/DD), the short carrier wavelength and large-area, square-law detector lead to efficient spatial diversity that prevents multipath fading. By contrast, radio links are typically subject to large fluctuations in received signal magnitude and phase. Freedom from multipath fading greatly simplifies the design of infrared links.

The infrared medium is not without drawbacks, however. Because infrared cannot penetrate walls, communication from one room to another requires the installation of infrared access points that are interconnected via a wired backbone. In many indoor environments there exists intense ambient infrared noise, arising from sunlight, incandescent lighting and fluorescent lighting, which induces noise in an infrared receiver. In virtually all short-range, indoor applications, IM/DD is the only practical transmission technique. The signal-to-noise ratio (SNR) of a direct-detection receiver is proportional to the square of the received optical power, implying that IM/DD links can tolerate only a comparatively limited path loss. Often, infrared links must employ relatively high transmit power levels and operate over a relatively limited range. While the transmitter power level can usually be increased without fear of interfering with other users, transmitter power may

Manuscript received October 10, 1996; revised December 12, 1996. This work was supported by National Science Foundation Grants ECS-9408957, ECS-9632829, and NCR-9308968, Hewlett–Packard, the University of California MICRO Program, IBM, and Siemens.

J. M. Kahn is with the Department of Electrical Engineering and Computer Sciences, University of California, Berkeley, CA 94720 USA (e-mail: jmk@eecs.berkeley.edu).

J. R. Barry is with the School of Electrical and Computer Engineering, Georgia Institute of Technology, Atlanta, GA 30332-0250 USA (e-mail: barry@ee.gatech.edu).

Publisher Item Identifier S 0018-9219(97)01832-X.

[1] In general, the infrared region includes wavelengths between about 700 nm and 100 μm. In this paper, unless otherwise noted, "infrared" refers to the near-infrared band between about 780 nm and 950 nm.

[2] In this paper, the term "radio" is inclusive of the frequency bands that are often referred to as "radio frequency," "microwave," and "millimeter wave."

Table 1 Comparison Between Radio and IM/DD Infrared Systems for Indoor Wireless Communication

Property of Medium	Radio	IM/DD Infrared	Implication for IR
Bandwidth Regulated?	Yes	No	Approval not required. Worldwide compatibility.
Passes Through Walls?	Yes	No	Less coverage. More easily secured. Independent links in different rooms.
Multipath Fading?	Yes	No	Simple link design.
Multipath Distortion?	Yes	Yes	
Path Loss	High	High	
Dominant Noise	Other Users	Background Light	Limited range.
Input $X(t)$ Represents	Amplitude	Power	Difficult to operate outdoors.
SNR Proportional to	$\int \lvert X(t)\rvert^2 dt$	$\int \lvert X(t)\rvert^2 dt$	Hight transmitter power requirement.
Average Power Proportional to	$\int \lvert X(t)\rvert^2 dt$	$\int X(t) dt$	Choose waveform $X(t)$ with high peak-to-average ratio.

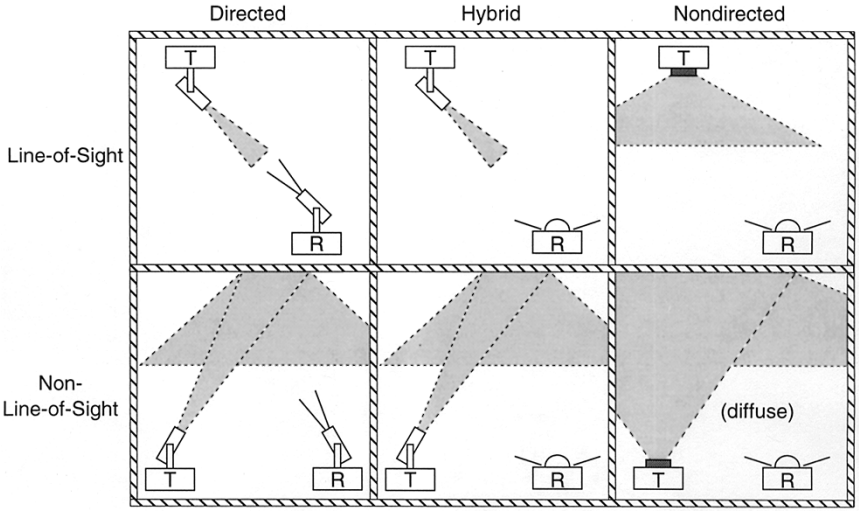

Fig. 1. Classification of simple infrared links according to the degree of directionality of the transmitter and receiver and whether the link relies upon the existence of a LOS path between them.

be limited by concerns of power consumption and eye safety, particularly in portable transmitters.

The characteristics of radio and infrared indoor wireless links are compared in Table 1.

Radio and infrared are complementary transmission media, and different applications favor the use of one medium or the other. Radio is favored in applications where user mobility must be maximized or transmission through walls or over long ranges is required and may be favored when transmitter power consumption must be minimized. Infrared is favored for short-range applications in which per-link bit rate and aggregate system capacity must be maximized, cost must be minimized, international compatibility is required, or receiver signal-processing complexity must be minimized.

B. Infrared Link Designs

Infrared links may employ various designs, and it is convenient to classify them according to two criteria. This classification scheme is shown in Fig. 1. The first criterion is the degree of directionality of the transmitter and receiver. *Directed links* employ directional transmitters and receivers, which must be aimed in order to establish a link, while *nondirected links* employ wide-angle transmitters and receivers, alleviating the need for such pointing. Directed link design maximizes power efficiency, since it minimizes path loss and reception of ambient light noise. On the other hand, nondirected links may be more convenient to use, particularly for mobile terminals, since they do not require aiming of the transmitter or receiver. It is also possible to establish *hybrid links*, which combine transmitters and receivers having different degrees of directionality.

The second classification criterion relates to whether the link relies upon the existence of an uninterrupted line-of-sight (LOS) path between the transmitter and receiver. *LOS links* rely upon such a path, while *non-LOS links* generally rely upon reflection of the light from the ceiling or some other diffusely reflecting surface. LOS link design maximizes power efficiency and minimizes multipath distortion. Non-LOS link design increases link robustness and ease of use, allowing the link to operate even when barriers, such as people or cubicle partitions, stand between the transmitter and receiver. The greatest robustness and ease of use are achieved by the nondirected-non-LOS link design, which is often referred to as a *diffuse link*.

C. IM/DD Channels

Modulation techniques for radio wireless systems include amplitude, phase, and frequency modulation (AM, PM, and FM), as well as some generalizations of these techniques [45]. Radio receivers employ one or more antennas, each followed by a heterodyne or homodyne down-converter, which is comprised of a local oscillator and a mixer. Efficient operation of this mixer relies upon the fact that it receives both the carrier and the local oscillator in a common electromagnetic mode. The down-converter output is an electrical signal whose voltage is *linear* in the amplitude of the received carrier electric field.

In a low-cost wireless infrared system, it is extremely difficult to collect appreciable signal power in a single electromagnetic mode. This spatially incoherent reception makes it difficult to construct an efficient heterodyne or homodyne downconverter for AM, PM, or FM, or to detect AM or PM by any other means. For infrared links, the most viable modulation is *intensity modulation* (IM), in which the desired waveform is modulated onto the instantaneous power of the carrier. The most practical down-conversion technique is *direct detection* (DD), in which a photodetector produces a current proportional to the received instantaneous power, i.e., proportional to the *square* of the received electric field.[3]

The modeling of infrared channels with IM/DD is illustrated in Fig. 2. The transmitted waveform $X(t)$ is the instantaneous optical power of the infrared emitter. The received waveform $Y(t)$ is the instantaneous current in the receiving photodetector, which is proportional to the integral over the photodetector surface of the total instantaneous optical power at each location. As indicated in Fig. 2(a), the received electric field generally displays spatial variation of magnitude and phase,[4] so that "multipath fading" would be experienced if the detector were smaller than a wavelength. Fortunately, typical detector areas are millions of square wavelengths, leading to spatial diversity that prevents multipath fading.[5] Thus when the detector is moved by a distance of the order of a wavelength, no change in the channel is observed. As the transmitted optical power $X(t)$ propagates along various paths of different lengths, infrared channels are still subject to multipath-induced distortion. As we will see, this distortion is most pronounced in links utilizing nondirectional transmitters and receivers, and especially when non-LOS propagation is employed. The channel can be modeled as a *baseband*

[3]It is possible to employ FM of the infrared source, and to use an optical filter to convert the received FM signal to an IM signal, which can then be directly detected. For detection of binary frequency-shift keying, this scheme can be made more efficient if the receiver employs two optical filters and two photodetectors. Nonetheless, it does not offer a performance gain over IM/DD. Moreover, with simple optical transmitters, it is difficult to obtain a frequency deviation sufficiently large that practical filters could be used for FM-IM conversion.

[4]Under very unusual circumstances, with point or plane-wave source, LOS propagation and carefully aligned detector, this spatial variation would exhibit a regular pattern, but in typical cases of LOS or diffuse propagation, it will appear random.

[5]The detector is equivalent to a two-dimensional array of many antennas whose receptions are squared, lowpass filtered, and summed.

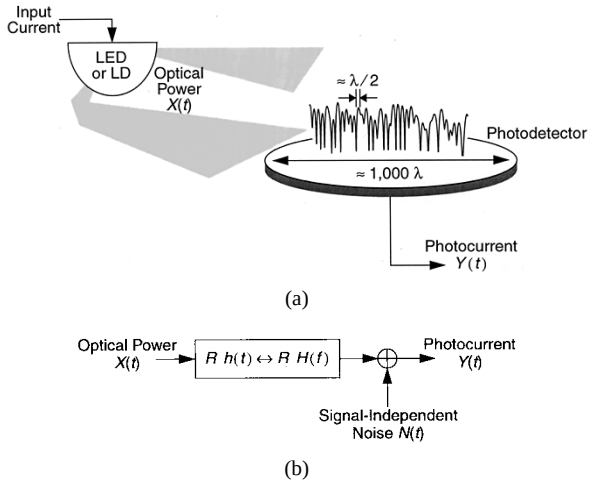

Fig. 2. (a) Transmission and reception in an infrared link with IM/DD. (b) Modeling link as a baseband linear, time-invariant system having impulse response $h(t)$, with signal-independent, additive noise $N(t)$. The photodetector has responsivity R.

linear system, with instantaneous input power $X(t)$, output current $Y(t)$, and an impulse response $h(t)$, as shown in Fig. 2(b). Alternately, the channel can be described in terms of the frequency response

$$H(f) = \int_{-\infty}^{\infty} h(t) e^{-j2\pi ft}\, dt$$

which is the Fourier transform of $h(t)$. It is usually appropriate to model the channel $h(t) \leftrightarrow H(f)$ as fixed, since it usually changes only when the transmitter, receiver, or objects in the room are moved by tens of centimeters. The linear relationship between $X(t)$ and $Y(t)$ is a consequence of the fact that the received signal consists of many electromagnetic modes [17]. By contrast, we note that when IM/DD is employed in dispersive single-mode optical fibers, the relationship between $X(t)$ and $Y(t)$ is sometimes nonlinear [46].

In many applications, infrared links are operated in the presence of intense infrared and visible background light. While received background light can be minimized by optical filtering, it still adds shot noise, which is usually the limiting noise source in a well-designed receiver (see Section II-F). Due to its high intensity, this shot noise can be modeled as white, Gaussian [47], and independent[6] of $X(t)$. When little or no ambient light is present, the dominant noise source is receiver preamplifier noise, which is also signal-independent and Gaussian (though often nonwhite). Thus we usually model the noise $N(t)$ as Gaussian and signal-independent. This stands in contrast to the signal-dependent, Poisson noise considered in photon-counting channel models. Fluorescent lamps emit infrared that is modulated in nearly periodic fashion; when present, this adds a cyclostationary component to $N(t)$. Ambient noise sources are discussed in detail in Section II-D.

[6]Because both signal and ambient light are received in many electromagnetic modes, $N(t)$ contains no significant signal-ambient cross terms.

Our baseband channel model is summarized by

$$Y(t) = RX(t) \otimes h(t) + N(t). \tag{1}$$

where the "$\otimes$" symbol denotes convolution and R is the detector responsivity (A/W). While (1) is simply a conventional linear filter channel with additive noise, infrared systems differ from conventional electrical or radio systems in several respects. Because the channel input $X(t)$ represents instantaneous optical power, the channel input is nonnegative:

$$X(t) \geq 0 \tag{2}$$

and the average transmitted optical power P_t is given by

$$P_t = \lim_{T \to \infty} \frac{1}{2T} \int_{-T}^{T} X(t)\, dt \tag{3}$$

rather than the usual time-average of $|X(t)|^2$, which is appropriate when $X(t)$ represents amplitude. The average received optical power is given by

$$P = H(0)P_t \tag{4}$$

where the channel dc gain is $H(0) = \int_{-\infty}^{\infty} h(t)\, dt$. As we will see in Sections II and IV, the performance of a digital link at bit rate R_b is related to the receiver electrical SNR[7]

$$\mathrm{SNR} = \frac{R^2P^2}{R_bN_0} = \frac{R^2H^2(0)P_t^2}{R_bN_0} \tag{5}$$

assuming that $N(t)$ is dominated by a white Gaussian component having double-sided power-spectral density N_0. From (5), we see that the SNR depends on the *square* of the received optical average power, implying that IM/DD infrared links must transmit at a relatively high power and can tolerate only a limited path loss. This stands in contrast to the case of conventional channels, where the SNR is proportional to the *first power* of the received average power.

D. Current Infrared Communication Systems

At present, most infrared links are of the directed-LOS or hybrid-LOS designs. The low path loss of these designs minimizes the transmitter power requirement and permits the use of a simple, low-cost receiver. Typically, these links transmit using a single light-emitting diode (LED), which emits an average power of several tens of mW that is concentrated within a semiangle of 15°–30°. The LED emission wavelength typically lies between 850 and 950 nm. This wavelength matches the responsivity peak of the silicon positive-intrinsic-negative (p-i-n) photodiode. In hybrid-LOS link designs, the photodiode is most often encapsulated in a planocylindrical or hemispherical plastic lens that serves to concentrate the received light, while maintaining a relatively wide field of view (FOV), e.g., a semiangle of the order of 60°. Directed-LOS links employ an optical concentrator that restricts the FOV, usually with the goal of providing a higher degree of optical concentration. Directed-LOS and hybrid-LOS links are relatively free from multipath distortion, sometimes permitting them to achieve bit rates above 100 Mb/s while maintaining a very simple design. These link designs are well suited for point-to-point and some point-to-multipoint applications, but are not suited for multiple-access networks, since it is difficult to establish full bidirectional connectivity between more than two transceivers.

Directed-LOS and hybrid-LOS links have been used for many years in remote-control units and other unidirectional, low-bit-rate applications. Over the past three years, the Infrared Data Association (IrDA) has established standards for short-range, half-duplex LOS links operating at bit rates up to 4 Mb/s [44]. Two of the key features of IrDA transceivers are low cost (well under $10) and low power consumption (under 1 W while transmitting, and under 100 mW when idle or receiving). At present, more than 130 companies worldwide are members of IrDA.

There are several key components of the IrDA standards [44]. The *IrDA Serial Infrared Physical Layer* defines standards for half-duplex links at several bit rates up to 4 Mb/s. 4 Mb/s links employ four-pulse-position modulation (4-PPM), while 1.152 Mb/s links utilize on-off keying (OOK) with return-to-zero (RZ) pulses having a duty cycle of 0.25. Links operating at bit rates of 115.2 kb/s and below employ OOK with RZ pulses having a duty cycle of 0.1875 (shorter pulses are permitted in some cases). IrDA-compliant transmitters must emit at a wavelength between 850 and 900 nm into a semiangle (at half-power) of 15°–30°. Compliant receivers must have a FOV (semiangle at half-effective light-collection area) of at least 15°. Most IrDA receivers have a much larger FOV, so that most IrDA links are of the hybrid-LOS type. IrDA links are required to achieve a bit error rate (BER) not exceeding 10^{-9} (10^{-8} for 4 Mb/s links) over a range of at least 1 m, but many links achieve a range as long as 3 m.

The *IrDA Infrared Link Access Protocol* (IrLAP) is derived from an existing asynchronous data communication standard, the high-level data-link control (HDLC) protocol. IrLAP utilizes most of the standard frame types defined by HDLC. IrLAP links may be point-to-point or point-to-multipoint. A key feature of IrLAP is that when a link is established, a negotiation process defines one node as primary, and all other nodes as secondary. All transmissions over the link must go to, or from, the primary node. IrLAP defines procedures for link initialization, device address discovery, connection start-up (including bit-rate negotiation), data exchange, disconnection, link shutdown, and device address conflict resolution.

The *IrDA Infrared Link Management Protocol* provides the means for multiple software applications running in each node to operate independently and concurrently, sharing the single link provided by IrLAP between the primary node and each secondary node. This involves three processes: discovery of the services that the link currently has available, multiplexing of the communications of several applications over the single link, and management of

[7] We define SNR in terms of average optical power to facilitate comparison of the average optical power requirements of different modulation techniques. Our definition of SNR differs from the conventional $\mathcal{E}_b/N_0$.

the link, including provision for applications that demand exclusive use of the link.

IrDA-standard transceivers are now an integral feature of numerous portable and fixed information appliances, including laptop computers, personal digital assistants, printers, and wireless access points to wired networks. It is also envisioned that IrDA transceivers will be incorporated into cellular and desktop telephones, pagers, watches, digital cameras, automobiles, public telephones, automatic teller machines, information kiosks, and industrial machinery, enabling new applications of short-range wireless communication.

Fig. 3(a)–(c) illustrate three general ways that IrDA-standard (or similar) links can be utilized (these three usage models are not mutually exclusive). In Fig. 3(a), a portable device (e.g., a laptop computer or personal digital assistant) establishes an infrared link to another portable device or to a fixed device (e.g., a desktop computer or printer). Typical applications include printing, file system synchronization, and "business card" exchange. In Fig. 3(b), a portable device establishes an infrared connection to an access point to a wired network (e.g., a networked desktop computer or a dedicated infrared access point). At present, both Extended Systems and Hewlett-Packard offer dedicated access points that bridge between IrDA links and Ethernet LAN's. Such access points make a wide range of networked applications available to portable devices. In the future, infrared access points in public telephones may enable wireless access to the Internet, while infrared links in automatic teller machines might allow one to download "digital cash."

As previously mentioned, links using directional, LOS transmitters, such as current IrDA links, cannot easily achieve full connectivity between more than two nodes, making them unsuitable for forming multiple-access networks. However, it might be possible to build a hub capable of establishing simultaneous point-to-point links with several portable devices, as illustrated in Fig. 3(c). Such a hub could be equipped with an internal switching fabric, buffering and control circuitry to interconnect the portables in a multiple-access LAN. At the same time, the hub could serve as a bridge to a wired network. For example, such a hub might be used for information exchange among several portables in a conference room. One technical challenge to building this hub is cochannel interference between different inbound transmissions. Since these transmissions will arrive from different directions, it might be possible to separate them using an angle diversity receiver. Angle diversity receivers are discussed in Section V below.

As mentioned previously, among all infrared link designs, diffuse links (nondirected-non-LOS links) are the most easy-to-use and robust, since no aiming of the transmitter or receiver is required, and since no LOS path between the transmitter and receiver is required. However, diffuse links have a higher path loss than their LOS counterparts, requiring higher transmit power and a receiver having a larger light-collection area. Typical diffuse transmitters employ several 850–900-nm LED's, which are sometimes oriented in different directions, to provide a diversity of propagation paths. When transmitting, they typically emit an average power in the range of 100–500 mW, making their power consumption higher than a typical IrDA transmitter. Diffuse receivers typically employ silicon p-i-n detectors encapsulated in hemispherical or plano-cylindrical lenses, which provide some light concentration while maintaining a wide FOV. Often they employ several detectors, in which case each is oriented in a different direction.

When several diffuse transceivers are located in proximity to each other, they naturally form a shared bus topology, making diffuse links suitable for multiple-access LAN's. However, "hidden nodes" may be present, i.e., each receiver cannot receive from, or even detect the presence of, each transmitter. When hidden nodes are present, random medium-access control (MAC) protocols that rely upon collision avoidance or detection, such as carrier-sense multiple access with collision detection (CSMA/CD) or with collision avoidance (CSMA/CA), do not always work reliably. Wireless LAN's using diffuse infrared can be formed in two different ways, which are illustrated in Fig. 3(d).

In the first technique, diffuse infrared links are used to achieve access to resources on a wired LAN. Clearly, this architecture also permits communication among the portable terminals via the wired backbone. This wireless LAN architecture is well suited for wireless data communication in offices, hospitals, schools, factories, restaurants, financial trading centers, or other heavily used environments, in which the cost of installing a backbone and wireless access points can be justified. An example of this type of wireless LAN is SpectrixLite^{TM}, made by the Spectrix Corporation. This system utilizes a base station to connect together up to 16 wireless access points, forming a LAN having an aggregate capacity of 4 Mb/s. The base station also bridges to a wired network (Ethernet or Token Ring). Portable terminals equipped with wireless LAN interfaces connect to the access points via 4 Mb/s links employing OOK with RZ pulses. These diffuse links are intended to achieve a BER of 10^{-6} over a range of 15 m. Transmission over the wireless LAN is controlled by the centralized, deterministic CODIAC protocol. Uplink bandwidth-reservation requests, uplink data and downlink data employ a single wavelength, and are time-division multiplexed together within a superframe interval. All transmissions occur at times scheduled by the CODIAC protocol, permitting portable transmitters and receivers to "sleep" at other times, thus saving power.

In the second technique, diffuse infrared links are employed to achieve direct, peer-to-peer communication between a number of portable and/or fixed terminals. This type of *ad hoc* interconnection is well suited to new or temporary work groups, for collaboration while traveling or at off-site meetings, or for setting up LAN's in a home or office environment in which all nodes are located within a single room. IBM supplies a diffuse infrared *ad hoc* LAN operating at 1 Mb/s using 16-PPM. It is intended to achieve coverage of a 10 m $\times$ 10 m region. The transceivers are

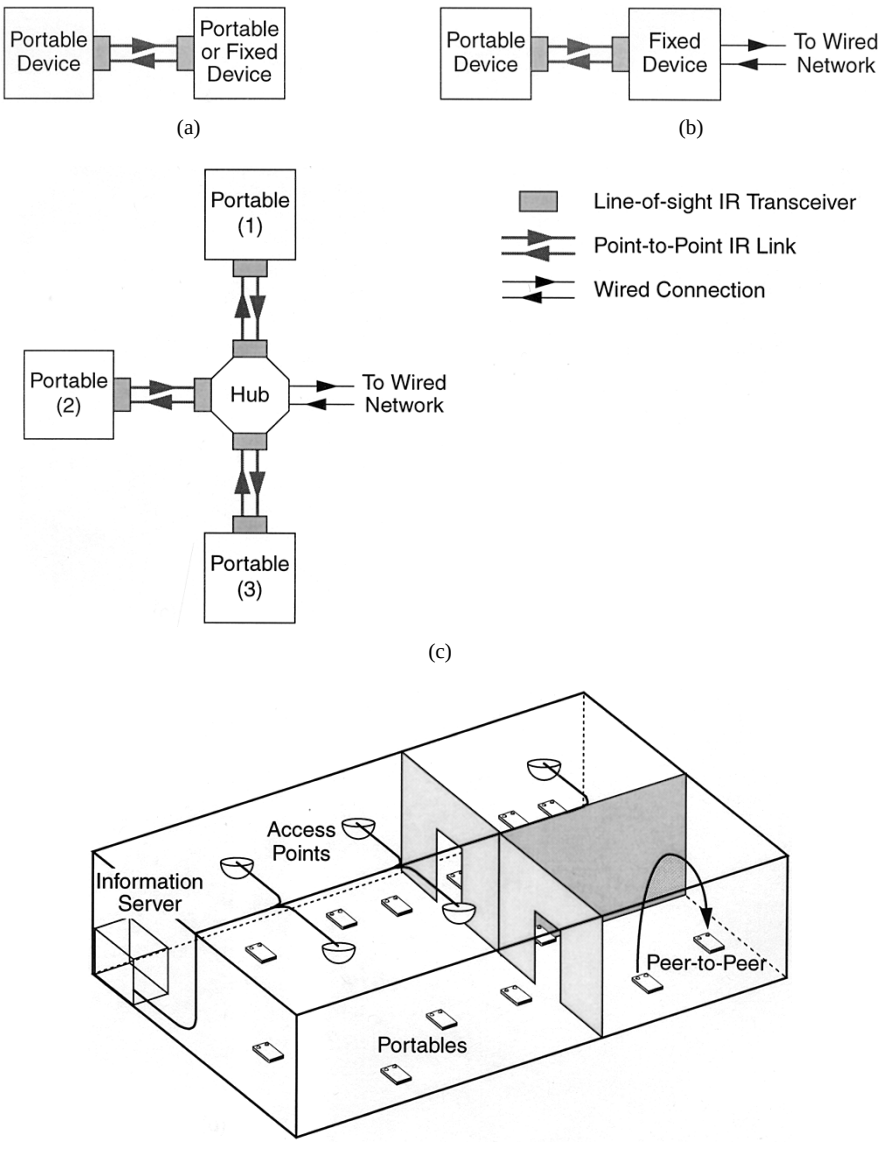

Fig. 3. Types of infrared wireless communication systems. (a) LOS, point-to-point (or point-to-multipoint) link, such as those standardized by the IrDA. (b) Point-to-point infrared link to a fixed device, which serves as a bridge to a wired network. (c) Hub capable of establishing simultaneous point-to-point links with several portable devices. The hub interconnects the portables in a multiple-access LAN, and bridges to the wired network. (d) LAN using diffuse, multiple-access links to connect portable devices to a wired network. A peer-to-peer connection of two portable devices is also shown.

not able to receive with high sensitivity while transmitting, so they cannot perform collision detection, and the LAN employs a CSMA/CA protocol. In order to perform collision avoidance, prior to initiating transmission, a transceiver listens to the shared channel. If the channel is free, it transmits a jam signal to reserve the channel, waits a time sufficient for all the stations to receive the jam signal, then transmits the payload packet. If acknowledgments indicate that a packet has been lost (usually due to a collision), the lost packet is retransmitted. When hidden nodes are present, collision avoidance can fail, causing the CSMA/CA protocol to crash. In this case, the IBM LAN changes the protocol to a deterministic, bandwidth-reservation scheme, which is stable, although it achieves lower throughput than CSMA/CA would in the absence of hidden nodes.

Through judicious use of the technologies employed in currently available systems, it is possible to enhance the performance of wireless infrared systems significantly. It appears likely that 10-Mb/s diffuse links and low-cost LOS links operating at tens of Mb/s can be achieved. Even higher bit rates will be desirable in future applications. Recent research work suggests that using new techniques, low-cost infrared links operating in the 100 Mb/s range may be achieved. In the remainder of this paper, we describe the nature of the infrared communication medium, obstacles to improved system performance and capacity, and the

Table 2 Comparison Between LED's and LD's (Shading Denotes an Advantage)

Characteristic	LED's	LD's
Spectral width	25–100 nm (10–50 THz)	$< 10^{-5}$ to 5 nm (< 1 MHz to 2 THz)
Modulation Bandwidth	Tens of kiloherz to tens of megahertz	Tens of kiloherz to tens of gigahertz
E/O Conversion Efficiency	10–20%	30–70%
Eye Safety	Generally considered eye-safe	Must be rendered eye-safe, especially for $\lambda < 1400$ nm
Cost	Low	Moderate to high

some of the means to overcome them. Section II describes how to achieve a high SNR, which is the single most difficult problem faced by the designer of an infrared link. Multipath distortion on infrared channels is characterized in Section III. Section IV provides a survey of various modulation techniques for infrared systems, comparing their power and bandwidth efficiencies, and characterizing their performance on multipath channels. In Section V, angle-diversity receivers and quasidiffuse transmitters are discussed. Multiple-access techniques are the subject of Section VI. Section VII describes an experimental 50-Mb/s diffuse infrared link, and Section VIII provides some concluding remarks.

II. Design of Power-Efficient Links

Achieving a high electrical SNR is the single biggest problem facing the designer of an infrared link. The difficulty arises for two reasons. Firstly, the SNR of an IM/DD link depends upon the square of the received optical average power. This implies that one should transmit at relatively high power, but available transmitter power may be limited by considerations of eye safety and power consumption. It also implies that one should design the link so as to minimize path loss and employ a receiver having a large light-collection area. Second, in many environments there exists intense ambient infrared noise, which introduces white shot noise and low-frequency cyclostationary noise into the receiver. This noise can be minimized through optical filtering and by employing a directional receiver, which can separate the desired signal from the ambient noise.

A. Infrared Transmitters and Eye Safety

The wavelength band between about 780 and 950 nm is presently the best choice for most applications of infrared wireless links, due to the availability of low-cost LED's and laser diodes (LD's), and because it coincides with the peak responsivity of inexpensive, low-capacitance silicon photodiodes. The primary drawback of radiation in this band relates to eye safety: it can pass through the human cornea and be focused by the lens onto the retina, where it can potentially induce thermal damage [49]. The cornea is opaque to radiation at wavelengths beyond about 1400 nm, considerably reducing potential ocular hazards, so that it has been suggested that the 1550-nm band may be better suited for infrared links. Unfortunately, the photodiodes presently available for this band, which are made of germanium or InGaAs, have much higher costs and capacitances per unit area than their silicon counterparts. To our knowledge, at present, all commercially available systems operate in the shorter-wavelength band.

Table 2 presents a comparison between LED's and LD's. LED's are currently used in all commercial systems, due to their extremely low cost and because most LED's emit light from a sufficiently large surface area that they are generally considered eye-safe. Typical packaged LED's emit light into semiangles (at half power) ranging from about 10°–30°, making them suitable for directed transmitters. Nondirected transmitters frequently employ multiple LED's oriented in different directions. Potential drawbacks of LED's include: 1) typically poor electro-optic power conversion efficiencies of 10–20% (though new devices have efficiencies as high as 40%), 2) modulation bandwidths that are limited to tens of MHz in typical low-cost devices, 3) broad spectral widths (typically 25–100 nm), which require the use of a wide receiver optical passband, leading to poor rejection of ambient light, and 4) the fact that wide modulation bandwidth is usually obtained at the expense of reduced electro-optic conversion efficiency.

LD's are much more expensive than LED's, but offer many nearly ideal characteristics: 1) electro-optic conversion efficiencies of 30–70%, 2) wide modulation bandwidths, which range from hundreds of MHz to more than 10 GHz, and 3) very narrow spectral widths (spectral widths ranging from several nm to well below 1 nm are available). To achieve eye safety with an LD requires that one pass the laser output through some element that destroys its spatial coherence and spreads the radiation over a sufficiently extended emission aperture and emission angle. For example, one can employ a transmissive diffuser, such as a thin plate of translucent plastic. While such diffusers can achieve efficiencies of about 70%, they typically yield a Lambertian radiation pattern, offering the designer little freedom to tailor the source radiation pattern. Computer-generated holograms [29] offer a means to generate custom-tailored radiation patterns with efficiencies approaching 100%, but must be fabricated with care to insure that any residual image of the LD emission aperture is tolerably weak.

The eye safety of infrared transmitters is governed by International Electrotechnical Commission (IEC) standards [49]. It is desirable for infrared transmitters to conform to the IEC Class 1 allowable exposure limit (AEL), implying that they are safe under all foreseen circumstances of use, and require no warning labels. At pulse repetition rates

higher than about 24 kHz, compliance with this AEL can be calculated on the basis of average emitted optical power alone. The AEL depends on the wavelength, diameter, and emission semiangle of the source. At present, the IEC is in the midst of revising the standards applying to infrared transmitters. Based on proposed revisions, at 875 nm, an IrDA-compliant source having an emission semiangle of 15° and diameter of 1 mm can emit an average power up to 28 mW. At the same wavelength, a Lambertian source (60° semiangle) having a diameter of 1 mm can emit up to 280 mW; at larger diameters, the allowable power increases as the square of the diameter.

B. Optical Filters and Concentrators

Infrared receivers typically employ either longpass or bandpass optical filters to attenuate ambient light. Longpass filters can be thought of as essentially passing light at all wavelengths beyond the cutoff wavelength.[8] They are usually constructed of colored glass or plastic, so that their transmission characteristics are substantially independent of the angle of incidence. Fig. 4(a) shows the transmission of a common longpass filter, superimposed upon the responsivity curve of a typical silicon photodiode. As the silicon device does not respond to wavelengths beyond about 1100 nm, the filter-photodiode combination effectively exhibits a bandpass optical response, whose bandwidth is several times that required to pass typical LED radiation. Longpass filters are used in almost all present commercial infrared systems.

Bandpass filters are usually constructed of multiple thin dielectric layers, and rely upon the phenomenon of optical interference [50]. These filters can achieve narrow bandwidths, leading to superior ambient light rejection (bandwidths below 1 nm are available commercially). In order to maximize the SNR, however, the transmitter optical spectrum must lie within the filter bandwidth, implying that when the filter bandwidth is made small, LD transmitters need to be used. The transmission spectrum of a typical bandpass filter is shown in Fig. 4(b). It is seen that the bandpass shifts to shorter wavelengths as one increases θ, the angle at which light strikes the filter. Such a filter must be used carefully if the receiver is intended to achieve a wide FOV.

An infrared receiver detects an optical power P that is proportional to its effective light-collection area. Increasing the photodiode area is expensive, and tends to decrease receiver bandwidth and increase receiver noise. Hence, it is desirable to employ an optical concentrator to increase the effective area. Concentrators may be of the imaging or nonimaging variety. The telescopes used in long-range, free-space optical links represent examples of imaging concentrators. Most short-range infrared links employ nonimaging concentrators.

[8]This is true within the band over which silicon detectors respond, though the filters do attenuate at still longer wavelengths.

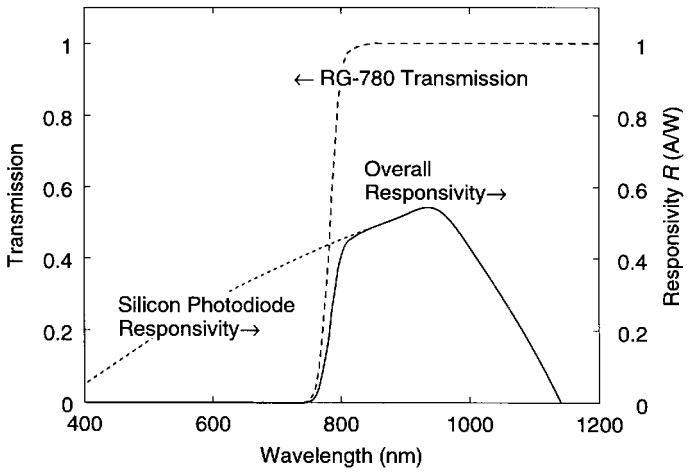

(a)

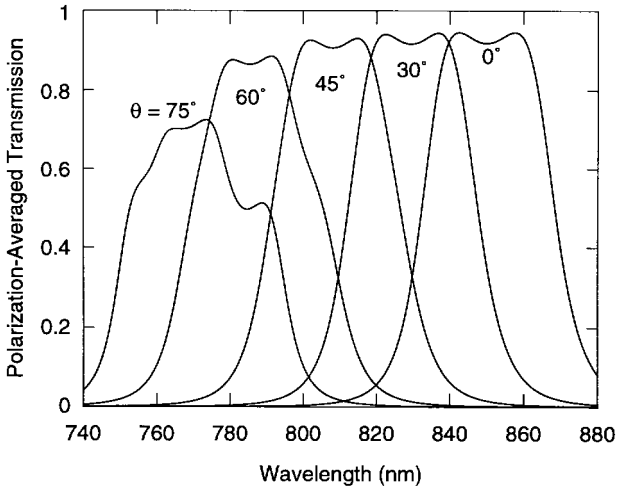

(b)

Fig. 4. (a) Responsivity of typical silicon p-i-n photodiode, transmission of typical longpass optical filter (Schott RG-780), and overall responsivity, which is the product of transmission and responsivity. (b) Polarization-averaged transmission of an optical bandpass filter for rays incident at angle θ. This filter is of a 25-layer, three-cavity design [10], [20].

Ignoring reflection losses, a bare detector achieves an effective signal-collection area of

$$A_{\text{eff}}^{\text{bare}}(\psi) = \begin{cases} A\cos\psi, & 0 \le \psi \le \pi/2 \\ 0, & \psi > \pi/2 \end{cases} \tag{6}$$

where A is the detector physical area and ψ is the angle of incidence with respect to the receiver axis. Adding a concentrator and filter, the effective signal-collection area becomes

$$A_{\text{eff}}(\psi) = \begin{cases} AT_s(\psi)g(\psi)\cos\psi, & 0 \le \psi \le \Psi_c \\ 0, & \theta > \Psi_c \end{cases} \tag{7}$$

where $T_s(\psi)$ is the signal transmission of the filter,[9] $g(\psi)$ is the concentrator gain and Ψ_c is the concentrator FOV

[9]$T_s(\psi)$ may represent an average over the filter transmission at different wavelengths (if the source spectrum is not narrow) and/or angles of incidence upon the filter (if different rays strike the filter at different angles of incidence). All losses arising from reflections, e.g., at the concentrator-detector interface) are included in $T_s(\psi)$.

(semiangle). Usually, $\Psi_c \leq \pi/2$. Nonimaging concentrators exhibit a trade-off between gain and FOV. An idealized nonimaging concentrator [51] having an internal refractive index n achieves a gain:

$$g(\psi) = \begin{cases} \dfrac{n^2}{\sin^2 \Psi_c}, & 0 \leq \psi \leq \Psi_c \\ 0, & \psi > \Psi_c. \end{cases} \tag{8}$$

From (8), we see that as the FOV is reduced, the gain within the FOV is increased.

The hemispherical lens is an important nonimaging concentrator [4], [16], [20], and is widely employed in commercial infrared systems [see Fig. 5(a) and (b)]. It achieves a wide FOV and omnidirectional gain, making it especially suitable for use in nondirected links. A hemisphere can achieve $\Psi_c \approx \pi/2$ and $g(\psi) \approx n^2$ over its entire FOV.[10] While this is sometimes called "omnidirectional gain," a hemisphere-based receiver is not truly omnidirectional, but has an effective area $A_{\text{eff}}(\psi) = An^2 \cos\psi$. When longpass filtering is employed, a planar longpass filter can be placed between the hemisphere and the detector, as shown in Fig. 5(a).

When bandpass filtering is utilized, it is not desirable to employ a planar filter in the configuration shown in Fig. 5(a). As ψ, the angle from which rays are received, shifts, so does θ, the angle at which light strikes the filter.[11] This shifts the filter passband, as described above, decreasing the filter transmission $T_s(\psi)$ for some ψ. Instead, as shown in Fig. 5(b), the bandpass filter should be deposited or bonded onto the outer surface of the hemispherical concentrator [16], [20]. Regardless of the angle ψ from which the signal is received, rays that reach the detector are incident upon the filter at small values of the angle θ, minimizing the shift of the filter passband, and maximizing its transmission. Thus with a hemispherical filter, it is possible to simultaneously obtain a narrow bandwidth and wide FOV.[12]

The compound parabolic concentrator (CPC) [51] is another nonimaging concentrator that is widely used in infrared links [12]. It can achieve much higher gain than the hemisphere, but at the expense of a narrower FOV, making it especially suitable for directed links. A CPC having FOV $\Psi_c < \pi/2$ can achieve a gain close to that given by (8). As shown in Fig. 5(c), a longpass or bandpass filter can be placed on the front surface of the CPC. The restricted FOV of a typical CPC is well matched to the restricted angular acceptance of a narrow bandpass filter. For example, a 30-nm-wide bandpass filter can be coupled with a CPC having a FOV $\Psi_c = 30°$ to achieve near-ideal performance [18]. Moreover, a second, inverted CPC can be placed in front of such a bandpass filter-CPC combination

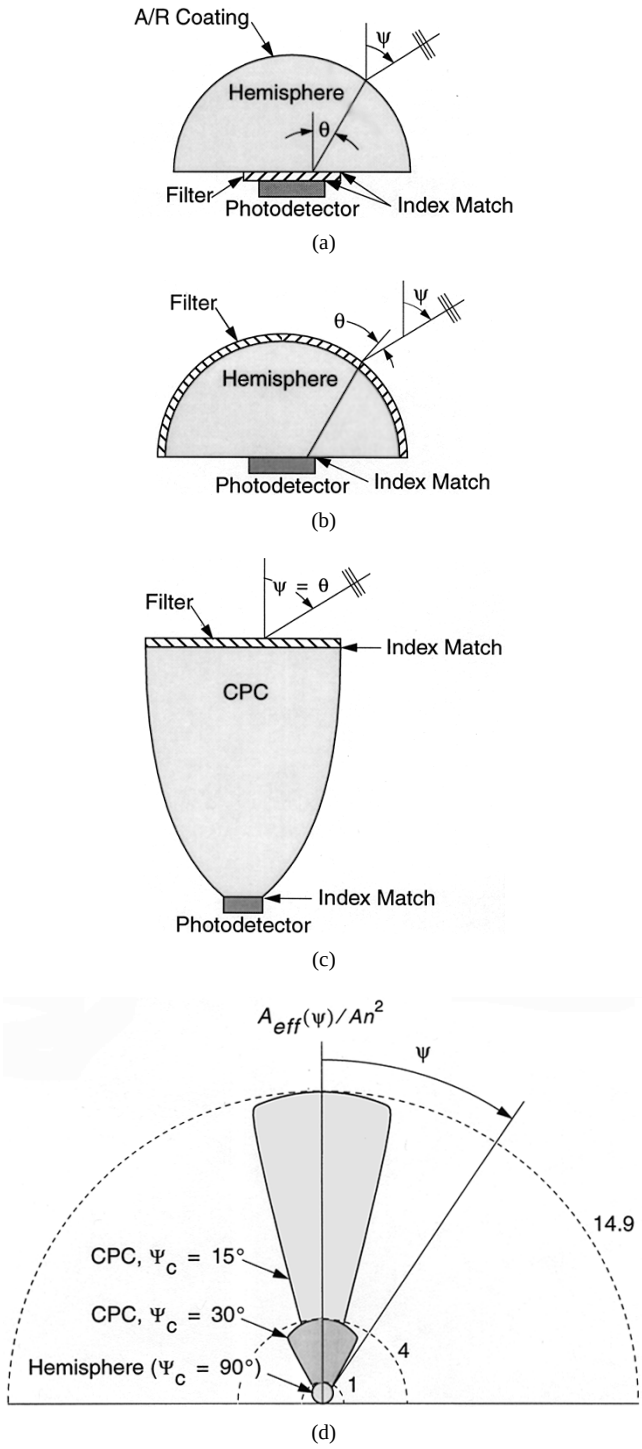

Fig. 5. Nonimaging optical concentrators: (a) hemisphere with planar optical filter, (b) hemisphere with hemispherical optical filter, (c) CPC with planar optical filter, and (d) effective light-collection areas achieved by ideal concentrators with lossless filters. Light rays are received from angle Ψ with respect to the receiver axis, and strike the filter at angle θ. The concentrator has a FOV (semiangle) Ψ_c and refractive index n, while the photodetector has area A.

[10] In order to achieve this, the hemisphere must be sufficiently large in relation to the detector, i.e., $R > n^2 r$, where r and R are the detector and hemisphere radii, respectively [10], [20].

[11] When light is incident at angle ψ across a broad area of the receiver, rays strike the filter over a range of θ that are close to ψ.

[12] Rays are incident upon the filter at angles $0 \leq \theta \leq \theta_{\max} = \sin^{-1}(nr/R)$, where r and R are the detector and hemisphere radii, respectively [10], [20]. Typically $\theta_{\max}$ is of the order of 30°. In order to choose a narrow filter bandwidth $\Delta\lambda$ that still achieves high $T_s(\psi)$, a reasonable procedure is to: 1) choose the filter center wavelength so that for $\theta = 0°$, the short-wavelength edge of the filter passband lies at the signal wavelength, and then 2) choose the filter bandwidth $\Delta\lambda$ so that for $\theta = \theta_{\max}$, the long-wavelength edge of the passband is at the signal wavelength. For example, the filter shown in Fig. 4(b) would result from this procedure for a signal wavelength of 840 nm and for $\theta_{\max} = 30°$.

to widen its input FOV to $\Psi_c \approx 90°$, while reducing the gain to n^2. Such a CPC-filter-CPC structure can achieve a wide FOV and narrow passband, but without requiring a hemispherical bandpass filter [18]. The principal drawback of CPC's is their excessive length, particularly for small Ψ_c. There exist more compact nonimaging concentrators that achieve performance near that of CPC's [52].

Fig. 5(d) compares the effective signal-collection areas achieved by ideal nonimaging concentrators with lossless filters, which have been computed using (7) and (8). The trade-off between FOV and gain is readily apparent.

It is important to note that a large fraction of the energy exiting a nonimaging concentrator does so at oblique angles, so that careful attention to antireflection coating and index matching at the concentrator-photodetector interface is required in order to achieve near-ideal performance.

C. Channel DC Gains

The frequency responses of infrared channels are relatively flat near dc, so for most purposes, the single most important quantity characterizing a channel is the dc gain $H(0)$,[13] which relates the transmitted and received average powers via (4). In this section we compute the dc gains of common link configurations (see Fig. 6).

In LOS links (either directed, hybrid, or nondirected), the dc gain can be computed fairly accurately by considering only the LOS propagation path. This approximation is particularly accurate in directed-LOS links. We consider the link geometry shown in Fig. 6(a). Suppose the transmitter emits an axially symmetric radiation pattern described by the radiant intensity (W/sr) $P_t R_o(\phi)$.[14] At the receiver, located at distance d and angle ϕ with respect to the transmitter, the irradiance $(\mathrm{W/cm^2})$ is $I_s(d,\phi) = P_t R_o(\phi)/d^2$. The received power is $P = I_s(d,\phi) A_{\mathrm{eff}}(\psi)$, and using (7), we obtain the channel dc gain:

$$H(0)_{\mathrm{LOS}} = \begin{cases} \dfrac{A}{d^2} R_o(\phi) T_s(\psi) g(\psi) \cos\psi, & 0 \le \psi \le \Psi_c \\ 0, & \theta > \Psi_c \end{cases} \tag{9}$$

which we observe is proportional to d^{-2}. From (9), we observe that if d and $R_o(\phi)$ are fixed, the most effective means to increase $H(0)$ are to increase the detector area A, and increase the concentrator gain $g(\psi)$ (by increasing the refractive index n and decreasing the FOV Ψ_c). Under some conditions, the power efficiency of a LOS link can be maximized by optimization of the transmitter radiant intensity $R_o(\phi)$ [10], [20]. For example, suppose the transmitter is pointed straight down from the ceiling, and as the receiver is moved about the room, it is pointed straight up at the ceiling. Then the condition $\psi \approx \phi$ is maintained. In this case, $R_o(\phi)$ can be enhanced at some values of ϕ to compensate for changes in $g(\psi)$, $T_s(\psi)$, and d as the receiver is moved.

[13] The channel has an optical path loss of $-10\log_{10} H(0)$ (measured in optical decibels), and an equivalent electrical dc gain of $10\log_{10} H^2(0)$ (measured in electrical decibels).

[14] Here, $R_o(\phi)$ is normalized so that $2\pi \int_0^{\pi} R_o(\phi)\sin\phi\, d\phi = 1$.

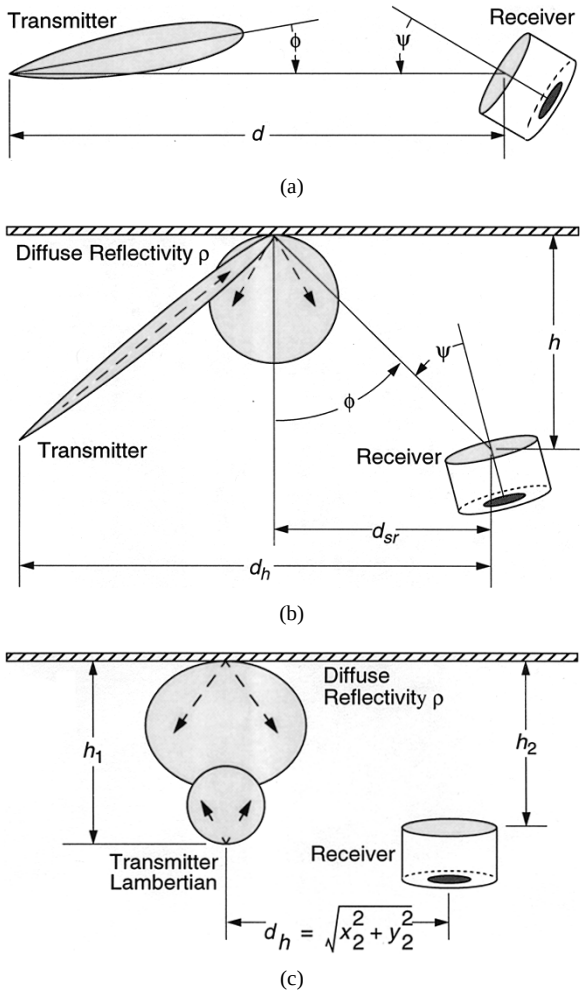

Fig. 6. Geometries used in channel gain calculations: (a) LOS, (b) directed-non-LOS or hybrid non-LOS, and (c) nondirected non-LOS (diffuse).

The emission from a variety of practical LOS transmitters can be modeled reasonably using a generalized Lambertian radiant intensity $R_o(\phi) = [(m+1)/2\pi]\cos^m\phi$ [1]. The order m is related to $\Phi_{1/2}$, the transmitter semiangle (at half power), by $m = -\ln 2/\ln(\cos\Phi_{1/2})$. For example, $\Phi_{1/2} = 60°$ (Lambertian transmitter) corresponds to $m = 1$, while $\Phi_{1/2} = 15°$ (typical directed transmitter) corresponds to $m = 20$. The channel dc gain is given by

$$H(0)_{\mathrm{LOS,Gen.Lamb.}} = \begin{cases} \dfrac{(m+1)A}{2\pi d^2} \cos^m\phi\, T_s(\psi) g(\psi) \cos\psi, & 0 \le \psi \le \Psi_c \\ 0, & \theta > \Psi_c. \end{cases} \tag{10}$$

If ϕ is kept very small, we can increase $H(0)$ by narrowing the transmitter semiangle $\Phi_{1/2}$, thereby increasing m.

Non-LOS infrared links exploit the fact that a wide variety of common building materials are efficient diffuse infrared reflectors. In the 800–900-nm range, typical plaster walls and acoustical ceiling tiles have diffuse reflectivities r in the range of 0.6–0.9, while darker materials often exhibit lower values of ρ [1], [17]. Most building materials (with the notable exception of glass) are approximately

Lambertian reflectors, i.e., they scatter light with a power per unit solid angle proportional to the cosine of the angle with respect to the surface normal, independent of the angle of incidence.[15]

To compute the gain of directed-non-LOS or hybrid-non-LOS channels, we refer to the geometry shown in Fig. 6(b). One of the principal advantages of this link design is that, assuming that the transmitter illuminates a fairly small region of the ceiling,[16] the channel gain depends only on d_{sr}, the horizontal separation between the illuminated spot and the receiver, not the transmitter-receiver horizontal separation d_h. If the ceiling of diffuse reflectivity ρ is located a distance h above the receiver, then the received signal irradiance is $I_s(d_{sr}, h) = \rho h P_t / \pi (h^2 + d_{sr}^2)^{3/2}$. The received power is $P = I_s(d_{sr}, h) A_{\text{eff}}(\psi)$, and the channel dc gain is

$$H(0))_{\text{directed-or hybrid-non-LOS}} = \begin{cases} \dfrac{\rho A h}{\pi (h^2 + d_{sr}^2)^{3/2}} T_s(\psi) g(\psi) \cos\psi, & 0 \le \psi \le \Psi_c \\ 0, & \theta > \Psi_c. \end{cases} \tag{11}$$

In directed-non-LOS or hybrid-non-LOS links, the most effective means to increase $H(0)$ are to increase the detector area A and the concentrator gain $g(\psi)$ (by increasing the refractive index n and decreasing the FOV Ψ_c).

To compute the dc gain of nondirected-non-LOS (diffuse) channels, one must consider the effect of multiple reflections from surfaces within the room. As a first-order approximation, we consider only the first bounce off of the ceiling [1], [3], and consider the configuration shown in Fig. 6(c). We will assume that the transmitter is pointed straight upward and emits a Lambertian pattern. We will also assume that the receiver is pointed straight upward, and employs a concentrator of FOV $\Psi_c \approx \pi/2$ that achieves omnidirectional gain $g(\psi) \approx g$ (typically $g \approx n^2$) and an omnidirectional filter having $T_s(\psi) \approx T_s$. The transmitter and receiver are located, respectively, at coordinates (0, 0) and (x_2, y_2) in the horizontal (x, y) plane. We integrate the power reflected from each ceiling element to obtain (see (12) at the bottom of the page). The most effective means to increase $H(0)$ are to increase the detector area A and the concentrator gain g (this should be done by increasing the refractive index n, but not by reducing the FOV Ψ_c). Equation (12) predicts that at large d_h, the channel gain $H(0)$ is expected to be proportional to d_h^{-4}. A diffuse link need not employ a Lambertian transmitter, and the increase of path loss with d_h can be made more gradual by employing several emitters angled in different directions [1], [32]. This strategy is employed in some commercial diffuse links.

[15] As shown in [1], for very large incidence angles (of order 70° and larger), even nominally diffuse reflectors exhibit a strong specular component.

[16] The diameter of the illuminated spot should be somewhat smaller than d_{sr}.

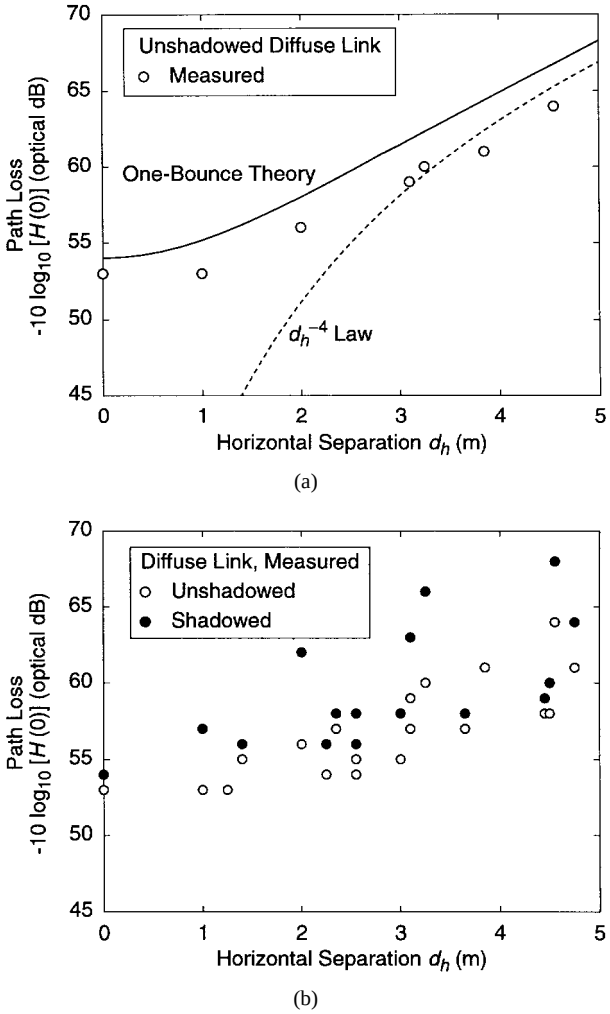

Fig. 7. Optical path loss of a diffuse infrared links employing a Lambertian transmitter and a detector of area $A = 1$ cm^2. (a) Measured in a single room having a ceiling of 80% diffuse reflectivity, for transmitter and receiver located 1.2 m and 1.6 m below the ceiling, respectively. (b) Measured in a collection of rooms, showing effect of shadowing at receiver [17].

Fig. 7(a) shows the path loss of a diffuse link, which was measured in a typical office [17]. The one-bounce theory (12) is reasonably accurate, but it underestimates $H(0)$ by a few decibels. Accurate prediction of $H(0)$ requires the inclusion of higher-order reflections (see the discussion of multipath channel simulation in Section III-B). For example, to model propagation in a large open office, for d_h exceeding about 5 m, reflections up to fifth order are required [11].

Fig. 7(b) presents the path losses of diffuse links mea-

$$H(0)_{\text{nondirected-non-LOS}} = \frac{\rho T_s g A h_1^2 h_2^2}{\pi^2} \cdot \iint_{\text{ceiling}} \frac{dx\, dy}{(h_1^2 + x^2 + y^2)^2 [(h_2^2 + (x - x_2)^2 + (y - y_2)^2]^2}. \tag{12}$$

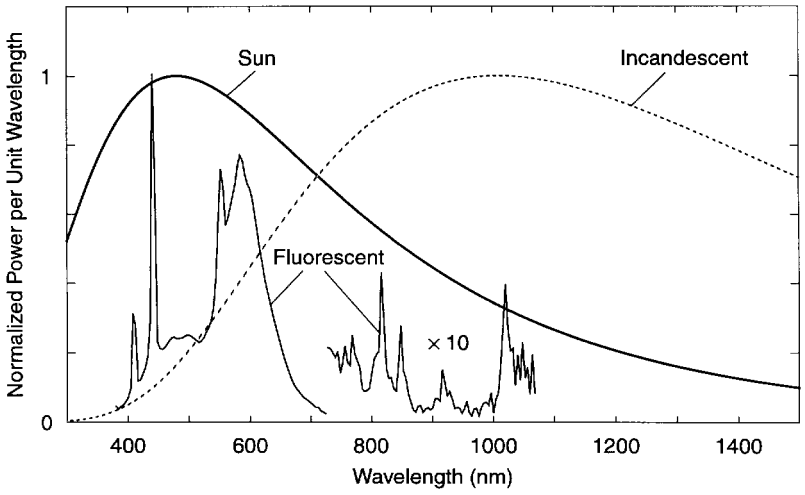

(a)

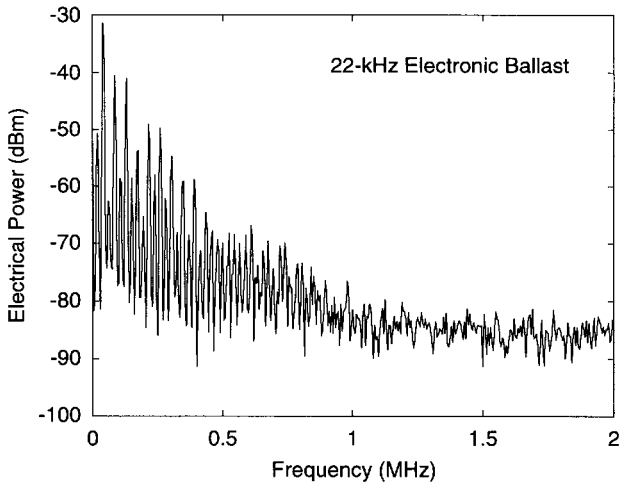

(b)

Fig. 8. (a) Optical power spectra of common ambient infrared sources. Spectra have been scaled to have the same maximum value. (b) Detected electrical power spectrum of infrared emission from a fluorescent lamp driven by a 22-kHz electronic ballast [38].

sured in several rooms [17]. In the unshadowed case, the propagation path was not blocked, while shadowing was effected by a person standing next to the receiver, so as to block the strongest propagation path (which was dominated by the first bounce off of the ceiling). In these diffuse links, shadowing decreased $H(0)$ by 2–5 dB. For comparison, we note that in nondirected-LOS links, shadowing was found to decrease $H(0)$ by 7–10 dB. This comparison illustrates the robustness of diffuse links against shadowing.

D. Ambient Light Noises

Many environments contain intense ambient infrared radiation arising from sunlight, skylight, incandescent and fluorescent lamps, and other sources [1], [41]. The optical power spectra of some common infrared sources are shown in Fig. 8(a).[17] Sunlight, skylight, and incandescent lamps represent essentially unmodulated sources[18] that can be received at an average power much larger than the desired signal, even when optical filtering is employed. The resulting dc photocurrent causes shot noise, which is a dominant noise source in typical infrared receivers, as shown below.

Here, we compute the optical power received from steady ambient light sources, which will be used to compute the shot noise they induce. We assume that the receiver employs a bandpass optical filter of noise bandwidth[19] $\Delta\lambda$ and peak transmission T_0. The ambient light noise is assumed to have a spectral irradiance p_n [$\mathrm{W/(cm^2}$ nm)] that is independent of wavelength within the filter bandwidth. If the ambient light originates from a localized source at angle ψ_n with respect to the receiver normal,[20] then the received ambient

[17] It should be emphasized that the power spectra in Fig. 8(a) have been normalized to have equal maximum value. Direct sunlight, when present, is typically much stronger than the other two sources.

[18] As shown in [41], incandescent lamps are modulated periodically at the power-line frequency, but because of their slow response time, this modulation contains few higher harmonics of that frequency.

[19] This noise bandwidth is generally close to, but slightly greater than, the 3 dB bandwidth of the filter.

[20] This is similar to the geometry of Fig. 6(a) or (b) but with the transmitter replaced by the noise source.

optical average power is

$$P_{n,\text{localized}} = p_n \Delta\lambda_n T_0 A g(\psi_n) \cos\psi_n. \quad (13)$$

If, instead, the ambient light is "isotropic"[21] and the receiver employs an ideal concentrator having a FOV Ψ_c, over which it achieves a constant gain given by (8), then the received ambient optical power is given by [10], [18]

$$P_{n,\text{isotropic}} = p_n \Delta\lambda_n T_0 A n^2. \quad (14)$$

We note that (14) is independent of the concentrator FOV Ψ_c. This occurs because as Ψ_c is varied, the gain (8) varies in such a way that the total received power P_n remains constant. If the concentrator is nonideal, (14) will overestimate P_n.

Fluorescent lamps emit strongly at spectral lines of mercury and argon that lie in the 780–950-nm band of interest for low-cost infrared systems. Fluorescent-lamp emission is modulated in a near-periodic fashion at the lamp drive frequency, and the detected electrical power spectrum contains discrete components at harmonics of the drive frequency. Traditionally, such lamps have been driven at the power-line frequency (50 or 60 Hz), and their electrical spectrum has contained energy at harmonics up to tens of kilohertz [3], [41]. However, recently introduced, high-efficiency "electronic ballasts" drive the lamps at frequencies of tens to hundreds of kilohertz. Their detected electrical spectrum contains energy up to hundreds of kilohertz [38], [41], making such lamps a potentially much more serious impairment to infrared links. Fig. 8(b) presents the detected electrical power spectrum from a lamp driven by a 22-kHz ballast. The system penalty caused by fluorescent-light noise depends strongly on the modulation scheme employed, so we defer discussion of this impairment until Section IV-D.

E. Photodetectors and Preamplifiers

As mentioned previously, the availability of low-cost, low-capacitance, large-area silicon photodiodes strongly favors choice of the 780–950 nm band over the region beyond 1400 nm for most infrared link applications. Two types of medium- and large-area silicon photodiodes are widely available: ordinary positive-intrinsic-negative (p-i-n) photodiodes and avalanche photodiodes (APD's) [53]. APD's are essentially p-i-n devices that are operated at very high reverse bias, so that photogenerated carriers create secondary carriers by impact ionization, resulting in internal electrical gain. APD's are favored in DD optical receivers when there is little ambient-induced shot noise, because their internal gain helps overcome preamplifier thermal noise, increasing the receiver SNR. APD-based receivers can lead to impressive infrared link performance when ambient light is weak [12]. When ambient-induced shot noise is dominant, however, use of an APD results in a net *decrease* in SNR [10], because the random nature of the APD's internal gain increases the variance of the shot noise by a factor greater than the signal gain. Additional drawbacks of APD's include their high cost, requirement for high bias, and their temperature-dependent gain. Ordinary silicon p-i-n photodiodes are employed in all commercial infrared links at present. We will restrict the remaining discussion to ordinary p-i-n photodiodes.

When it receives an instantaneous optical power $p(t)$, a p-i-n photodiode produces an instantaneous photocurrent $i(t) = Rp(t)$, where the *responsivity* is R (A/W). The responsivity of a typical silicon p-i-n photodiode is shown in Fig. 4(a), and is seen to peak near 950 nm. We assume that the desired signal and ambient light are received with average optical powers P and P_n, respectively. Assuming that $P_n \gg P$, the ambient light induces in the detector a shot noise current $N_{\text{shot}}(t)$, which is essentially white, Gaussian, and independent of the desired signal,[22] and which has a one-sided power-spectral density (PSD):

$$S_{\text{shot}}(f) = 2qRP_n \quad (15)$$

where q is the electronic charge. $S_{\text{shot}}(f)$ has units of A^2/Hz.

Among preamplifier designs, the transimpedance type is best suited to most infrared link applications, because its achieves a large dynamic range and a wide bandwidth without the need for equalization [54]. Under typical conditions, lower noise is achieved if the front-end device is a field-effect transistor (FET), rather than a bipolar-junction transistor (BJT) [22], [54]. If power consumption is constrained, however, a BJT may achieve superior results [22]. We will assume the use of a FET-based transimpedance preamplifier. A simplified schematic of such a circuit is shown in Fig. 9(a). Assuming that the amplifier of gain A_2 is ideal, the circuit has a single-pole response with cutoff frequency $f_{-3\text{dB}} = (g_m R_d A_2 + 1)/(2\pi R_F C_T)$. In infrared receivers, the total input capacitance $C_T = C_d + C_{gs} + C_{gd}$ is usually dominated by the detector capacitance C_d, because of the large detector area required to achieve a high SNR. The total input-referred noise PSD of this preamplifier is

$$S_{\text{total}}(f) = S_{\text{shot}}(f) + S_{\text{thermal}}(f) \quad (16)$$

where the dominant contributions to the input-referred thermal noise PSD are given by

$$S_{\text{thermal}}(f) = \frac{4kT}{R_F} + \frac{16\pi^2 kT}{g_m}\left(\Gamma + \frac{1}{g_m R_D}\right) C_T^2 f^2 + \frac{4\pi^2 K I_D^a C_T^2 f}{g_m^2}. \quad (17)$$

Here, k is Boltzmann's constant, T is absolute temperature, Γ is the FET channel noise factor, K and a are the FET $1/f$ noise coefficients, and I_D is the FET drain current. These PSD's are plotted in Fig. 9(b), assuming parameters that might be typical of a receiver operating in a 10-Mb/s diffuse link. The first term in (17) is a white noise arising from the

[21] More precisely, it is received with equal radiant intensity for $0 \le \psi \le \pi/2$.

[22] Although the desired signal does contribute to this shot noise, it is usually not important to include this contribution, even when $P_n = 0$, because it is typically much smaller than the preamplifier thermal noise.

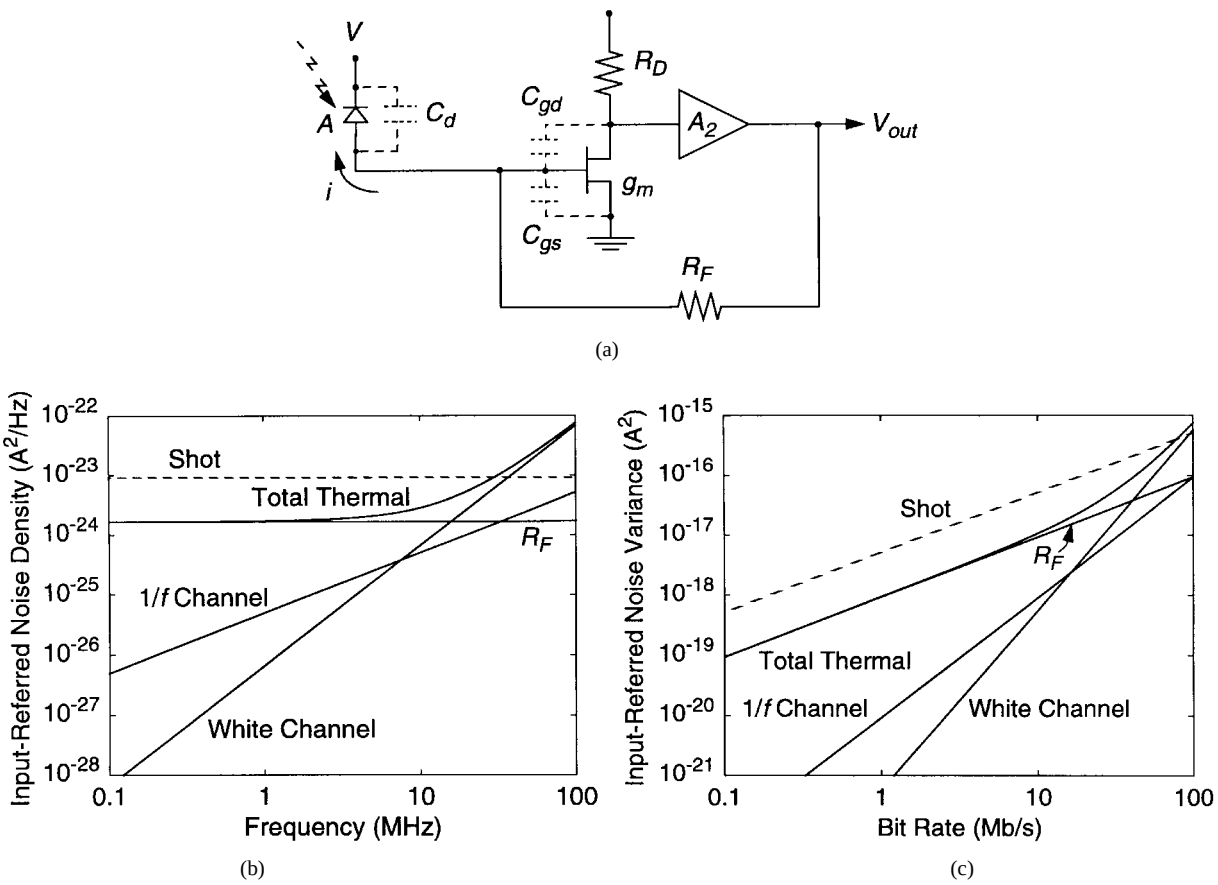

Fig. 9. (a) Simplified schematic of FET-based transimpedance preamplifier. (b) Dominant input-referred noise power spectral densities (one-sided). (c) Dominant input-referred noise variances. Parameters assumed in (b) and (c) include: isotropic bright skylight of spectral irradiance $p_n = 6\ \mathrm{mW/(cm^2\ nm)}$, optical filter noise bandwidth $\Delta\lambda_n = 30$ nm, and optical concentrator noise gain $g = 3$. The p-illuminated silicon p-i-n photodetector has area $A = 0.1\ \mathrm{cm}^2$, responsivity $R = 0.53$ A/W, depletion width $w = 60$ mm, capacitance $C_d = 17.5$ pF, and reverse bias $V = 30$ V. The ambient-induced dc photocurrent is $I_{dc} = 28.6$ mA. The feedback resistance is $R_F = 10$ kΩ. The FET parameters are $g_m = 40$ mS, $C_{gs} + C_{gd} = 1.0$ pF, $f_T = 6.4$ GHz, $I_D = 20$ mA, $K = 294$ fA, $a = 1$.

feedback resistor R_F and is minimized by choosing R_F as large as possible, while still achieving a sufficiently large preamplifier cutoff frequency.[23] The second term in (17) arises from the FET white channel noise. It increases as f^2, so that it tends to become the dominant noise source in receivers for very high bit rates. This term is minimized by minimizing the total input capacitance C_T. Because C_T is often dominated by the detector capacitance C_d, this often amounts to minimizing C_d. The second term is also minimized by choosing an FET having a transconductance g_m as high as possible, subject to constraints on power consumption. The third term in (17) is proportional to f, so that it also becomes important at high bit rates. It arises from the FET $1/f$ channel noise and is minimized through choice of small C_T, high g_m, and an FET type having small K.

A typical p-i-n photodiode is illuminated through either the p or n contact and has a capacitance given by $C_d = \varepsilon A/2$, where A is the device area, w is the depletion-layer thickness, and ε is the semiconductor permittivity. For high-bit-rate receivers, in which the second two terms of (17) become important, this seems to imply that w should be chosen as large as possible. It should be noted, however, that increasing w eventually leads to transit-time limitations in the photodetector frequency response [53]. Simple considerations show that for photodiodes much thicker than the photon absorption length and at electric fields well below saturation, the transit-time-limited cutoff frequency is approximately proportional to $\mu V/w^2$, where μ is the mobility of the carrier type that is collected by the contact opposite the illuminated contact, and V is the photodiode reverse bias. Fig. 10 shows the theoretically calculated transit-time-limited frequency response of silicon p-i-n photodiodes illuminated through the p and n contacts. The p-illuminated photodiode has a much wider bandwidth than the n-illuminated device, since electrons have a mobility much higher than holes. It has been shown that when a constraint is placed on the bias voltage V, receiver performance is optimized when w is chosen so that the transit-time-limited 3-dB cutoff approximately equals the bit rate (assuming OOK modulation) [22]. Metal-semiconductor

[23] For OOK with nonreturn-to-zero (NRZ) pulses, a cutoff frequency equal to the bit rate is typically required.

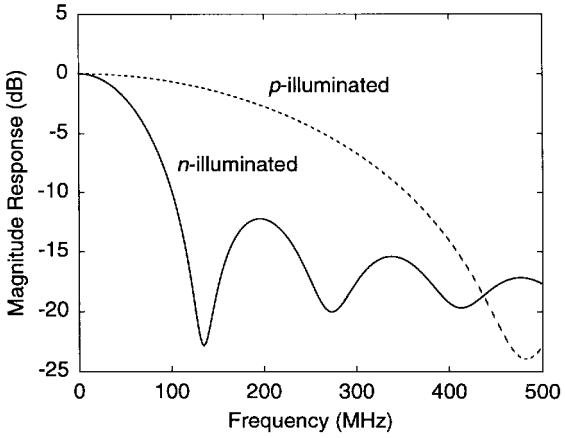

Fig. 10. Transit-time-limited frequency responses of silicon p-i-n photodiodes illuminated through the n- and p-doped contacts. Responses have been normalized to 0 dB at dc. These responses assume: depletion width $w = 100$ mm, reverse bias $V = 30$ V, uniform electric field in depletion region, and absorption coefficient $\alpha = 103\ \mathrm{cm}^{-1} (\lambda = 800$ nm).

metal (MSM) photodiodes have a different relationship between capacitance and transit time than conventional p-i-n photodiodes, owing to their different geometry. While MSM detectors can yield improved performance in optical-fiber receivers [56], analysis suggests that an improvement is not likely in very large-area infrared receivers [22].

F. Receiver SNR and BER

In this section we compute the receiver SNR and BER. We assume here that the receiver transmits at bit rate R_b using on–off keying (OOK) with NRZ pulses. The transmitted average power is P_t, and the received average power is $P = H(0)P_t$, where the channel dc $H(0)$ gain can be computed as in Section II-C above. We assume that the channel is distortionless, i.e., it has a gain $H(f) = H(0)$ for all frequencies of interest. Following [55], at the receiver, the preamplifier is followed by an equalizer that converts the received pulse to one having a raised-cosine Fourier transform with 100% excess bandwidth. The equalizer gain is chosen so that when sampled, its output is either zero or $2RP$ (A), ignoring noise. Each sample of the equalizer output contains a Gaussian noise having a total variance (A^2) that is the sum of contributions from shot and thermal noises

$$\sigma^2_{\mathrm{total}} = \sigma^2_{\mathrm{shot}} + \sigma^2_{\mathrm{thermal}}. \tag{18}$$

The SNR is expressed as

$$\mathrm{SNR} = \frac{(RP)^2}{\sigma^2_{\mathrm{total}}} \tag{19}$$

and the BER is given by $\mathrm{BER} = Q(\sqrt{\mathrm{SNR}})$, where

$$Q(x) = \frac{1}{\sqrt{2\pi}} \int_x^\infty e^{-y^2/2}\, dy.$$

For example, to achieve $\mathrm{BER} = 10^{-9}$ requires $\mathrm{SNR} = 15.6$ dB. The shot-noise variance is given by

$$\sigma^2_{\mathrm{shot}} = 2qRP_nI_2R_b \tag{20}$$

while the thermal-noise variance is given by

$$\sigma^2_{\mathrm{thermal}} = \frac{4kT}{R_F} I_2 R_b + \frac{16\pi^2 kT}{g_m}\left(\Gamma + \frac{1}{g_m R_D}\right) C_T^2 I_3 R_B^3 + \frac{4\pi^2 K I_D^a C_T^2}{g_m^2} I_f R_b^2. \tag{21}$$

We have defined the noise-bandwidth factors $I_2 = 0.562$, $I_3 = 0.0868$, and $I_f = 0.184$. Examining (20) and (21), we see that the shot noise and R_F noise, which have white input-referred PSD's, lead to variances proportional to the bit rate R_b. The FET white channel noise and $1/f$ channel noise, with input-referred PSD's proportional to f^2 and f, lead to variances proportional to R_b^3 and R_b^2, respectively. The various terms in the noise variances (20) and (21) are plotted as a function of bit rate Fig. 9(c). For the parameters considered there, which might be typical of a 10-Mb/s diffuse receiver, shot noise is dominant up to a bit rate of tens of Mb/s, above which the white channel noise becomes the leading term.

Examining the SNR (19), we note that the numerator is always proportional to the square of the detector area, i.e., A^2. We note that the shot noise variance (20) is always proportional to the detector area, A. Hence, if shot noise is the dominant noise source, then the SNR is proportional to the detector area, i.e., $\mathrm{SNR} \propto A$. The thermal noise variance (21) is a complicated function of A, and is only independent of A if the R_F term is always dominant. When the R_F noise is the dominant noise source, then the SNR is proportional to the square of the detector area, i.e., $\mathrm{SNR} \propto A^2$.

Fig. 11 illustrates the average transmitter power P_t required to achieve 10^{-6} BER in nondirected-LOS links [10], [20]. These links operate in the presence of bright skylight, and shot noise is assumed to be the dominant noise source. This example considers the use of a hemispherical concentrator, and compares the performance of bandpass filters in planar and hemispherical geometries [as shown in Fig. 5(a) and (b)]. The transmitter is placed at ceiling height in the center of the cell. For each cell radius, the optical filter bandwidth and center wavelength are optimized jointly with the transmitter radiation pattern so as to minimize the transmitter power required to achieve the desired BER everywhere within the cell. Use of the hemispherical filter reduces the transmitter power requirement by about 3 dB over the planar filter. This occurs because only the hemispherical filter is able to achieve simultaneously a narrow bandwidth and high signal transmission over a wide FOV. We note that if the link were to employ PPM instead of OOK, the transmitter power requirements could be further reduced by several dB (see Section IV).

III. Multipath Distortion in Nondirected Links

While nondirected propagation alleviates the need for physical alignment between the transmitter and the receiver, a major drawback of this approach is the signal distortion caused by reflections from ceilings, walls, and other objects. In this section, we describe experimental characterization of

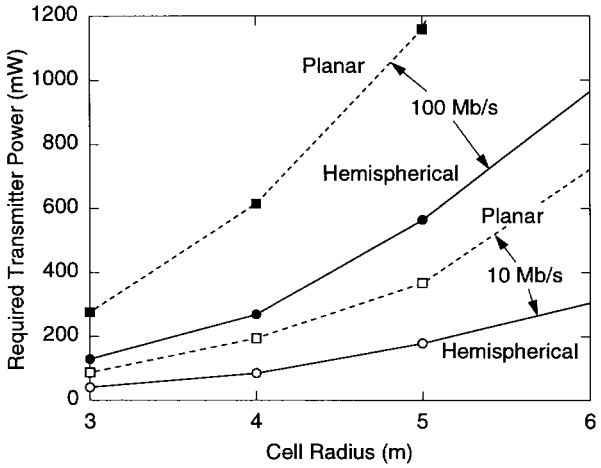

Fig. 11. Average transmitter power required to achieve 10^{-6} BER using OOK in nondirected-LOS links, comparing planar and hemispherical bandpass filters. The transmitter is placed at ceiling height in the center of the cell. Shot noise induced by skylight is the dominant noise source. The detector area is $A = 1\ \mathrm{cm}^2$, and the hemispherical concentrator has a 2-cm radius and refractive index $n = 1.7$. For each cell radius, the bandpass filter bandwidth and center wavelength are optimized jointly with the transmitter radiation pattern. For example, at a 5-m cell radius, the optimized planar and hemispherical filters have bandwidths of 70.6 nm and 10.7 nm, respectively [10], [20].

multipath channels, as well as techniques to simulate and model them. In Section IV, we will quantify the penalties that multipath distortion causes in very high-bit-rate links.

A. Experimental Results

Two experimental studies have characterized multipath distortion in nondirected links, obtaining similar results [13], [17]. In [17], we employed a vector network analyzer to perform swept-modulation-frequency characterization [48] of the channel frequency response $H(f)$. The 832-nm transmitter emitted a Lambertian radiation pattern. During all measurements, the receiver was placed at desk height and pointed upwards. To form nondirected-LOS configurations (referred to in this section simply as "LOS"), the transmitter was placed near the ceiling and pointed straight down, while for nondirected-non-LOS (diffuse) configurations, it was placed at desk height and pointed straight up. The channel impulse response $h(t)$ was obtained by inverse Fourier transformation of $H(f)$.

Fig. 12 presents the magnitude and impulse responses of four different nondirected link configurations, measured in an empty conference room. While the details of channel responses depend on the link geometry, responses measured at all positions in all rooms exhibit qualitative similarity to Fig. 12. Unshadowed LOS impulse responses are dominated by a short initial pulse, and the strongest distinct reflections typically arrive 15–20 ns after the initial pulse. Dominance of the short initial pulse leads to magnitude responses that are flat at high frequencies. Unshadowed diffuse impulse responses exhibit a significantly wider initial pulse, which has a width of about 12 ns at 10% height, corresponding to the existence of a continuum of different path lengths between illuminated portions of the

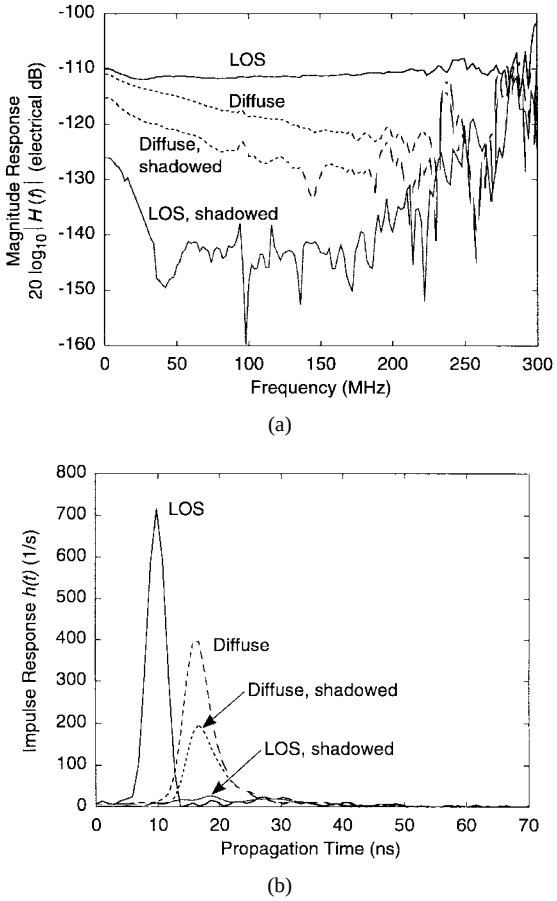

Fig. 12. Responses of nondirected-LOS and nondirected-non-LOS (diffuse) channels. Measurements were performed in a 5.5 m × 7.5 m room having a 3.5-m-high ceiling. Shadowing was effected by a person standing next to receiver. Detector area was $A = 1\ \mathrm{cm}^2$. (a) Frequency responses. (b) Impulse responses obtained by inverse Fourier transformation of the frequency responses using a 300-MHz Hamming window [17].

ceiling and the receiver. This continuous distribution of path delays leads to a steady decrease in the channel magnitude response at high frequencies. For all channels, the impulse response may contain significant energy as long as 70 ns after its initial nonzero excursion. The dc gain of all channels is enhanced over that at high frequencies, because it includes the contribution due to the entire duration of the impulse response.

Shadowed channels exhibit characteristics that are slightly less predictable than the unshadowed channels. The shadowed LOS impulse response typically resembles the corresponding unshadowed response with the dominant initial pulse removed, since only indirect propagation paths remain. We observe that in LOS configurations, shadowing significantly degrades the channel frequency and impulse responses. Diffuse configurations are far less vulnerable to shadowing than their LOS counterparts, because in diffuse configurations there exist many possible propagation paths between the illuminated ceiling area and the receiver. In diffuse configurations, shadowing produces a slight broadening of the impulse response, and a slight increase in the rate of rolloff of the magnitude response with increasing frequency.

A useful measure of the severity of intersymbol interference (ISI) induced by a multipath channel $h(t)$ is the channel root-mean-square (rms) delay spread D. As shown in Section IV, the delay spread of a channel is a remarkably accurate predictor of ISI-induced SNR penalties, independent of the particular time dependence of that channel's impulse response. The delay spread is computed from the impulse response using

$$D = \left[\frac{\int_{-\infty}^{\infty} (t-\mu)^2 h^2(t)\, dt}{\int_{-\infty}^{\infty} h^2(t)\, dt} \right]^{1/2} \tag{22}$$

where the mean delay μ is given by

$$\mu = \frac{\int_{-\infty}^{\infty} t h^2(t)\, dt}{\int_{-\infty}^{\infty} h^2(t)\, dt}. \tag{23}$$

The impulse response $h(t)$ and delay spread D can be considered to be deterministic quantities, in the sense that as long as the positions of the transmitter, receiver and intervening reflectors are fixed, $h(t)$ and D are fixed. This stands in contrast to the case of time-varying radio channels, where the rms delay spread is interpreted as a statistical expectation of a random process [48].

Fig. 13(a) and (b) present the rms delay spread versus horizontal separation for measured multipath channels [17]. In the absence of shadowing, LOS channels, whose impulse response is dominated by a short initial pulse, generally yield the smallest delay spreads, ranging from a measurement-limited 1.3 ns to about 12 ns. Unshadowed diffuse channels exhibit delay spreads that lie in the same range, but which are systematically slightly larger, due to the finite temporal spread of the dominant reflection from the ceiling. Shadowing increases the delay spread of both LOS and diffuse channels but, as might be expected, the increase is relatively modest for the latter channels. Shadowed LOS channels consistently exhibit the largest delay spreads, typically between 7 and 13 ns.

B. Simulation and Modeling

Simulation techniques for radio multipath channels frequently assume specular reflection and employ "ray tracing." By contrast, infrared multipath propagation is usually dominated by diffuse reflection, a process in which the energy reflected from each surface element follows a Lambertian distribution, independent of the angle of incidence. We have developed a technique to simulate multipath infrared propagation, which can account for an arbitrary number of diffuse reflections from room surfaces [9], [10]. This technique is based on the observation that given a particular source $\mathcal{S}$ and receiver $\mathcal{R}$ in a room with reflectors, light from the source can reach the receiver after any number of reflections. Therefore, the impulse response can

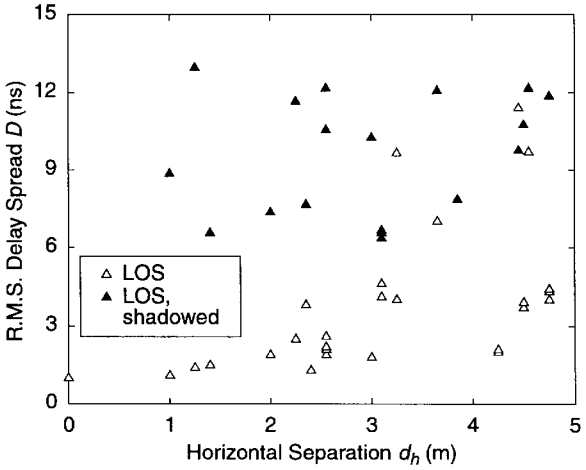

(a)

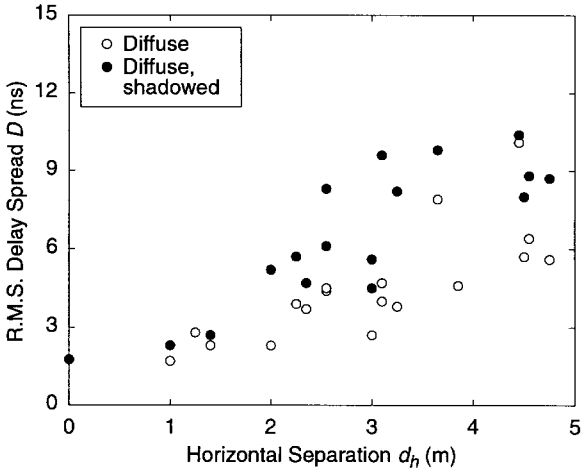

(b)

Fig. 13. RMS delay spreads of (a) nondirected-LOS and (b) nondirected-non-LOS (diffuse) channels. Shadowing was effected by a person standing next to receiver [17].

be written as an infinite sum:

$$h(t;\mathcal{S},\mathcal{R}) = \sum_{k=0}^{\infty} h^{(k)}(t;\mathcal{S},\mathcal{R}) \tag{24}$$

where $h^{(k)}(t)$ is the response of the light undergoing *exactly* k reflections. Reflecting surfaces in the room are divided into small elements, $\mathcal{E}_i, 1 \le i \le N$. The LOS response $h^{(0)}(t)$ between $\mathcal{S}$ and $\mathcal{R}$ is computed first. Each higher-order term $h^{(k)}(t), k>0$, is then calculated recursively from $h^{(k-1)}(t)$:

$$h^{(k)}(t;\mathcal{S},\mathcal{R}) = \sum_{i=1}^{N} h^{(0)}(t;\mathcal{S},\mathcal{E}_i) \otimes h^{(k-1)}(t;\mathcal{E}_i,\mathcal{R}). \tag{25}$$

Examining (25), we see that each reflecting element $\mathcal{E}_i$ makes a contribution to the k-bounce response $h^{(k)}(t)$ that is composed of the LOS response from the source $\mathcal{S}$ to element $\mathcal{E}_i$, convolved with the $(k-1)$-bounce response between that reflecting element and the receiver. Fig. 14 illustrates the simulation of a diffuse infrared channel. The individual contributions from bounces $k = 1, 2, 3$ are shown

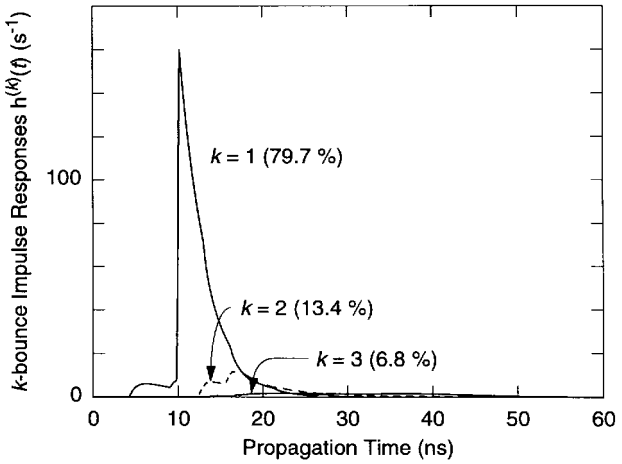

(a)

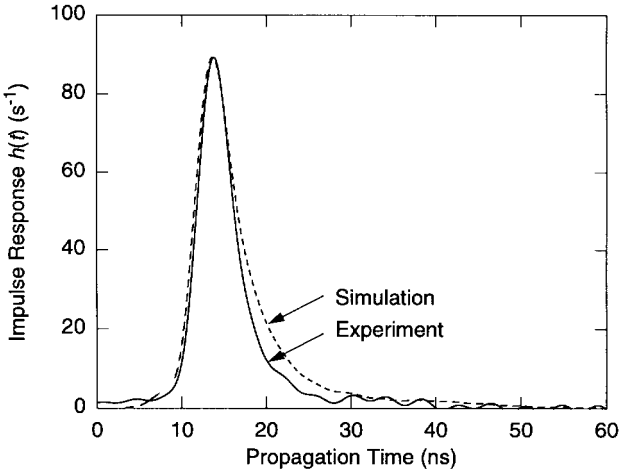

(b)

Fig. 14. Simulation of a multipath propagation in a diffuse link. (a) Contributions to impulse response from light that has undergone k bounces for $k = 1, 2, 3$. (b) Comparison of simulation to experiment. In (b), the simulated impulse response has been convolved with the impulse response of the experimental measurement system [9], [10].

in Fig. 14(a). The term $k = 0$ is absent, as there is no direct LOS path between the transmitter and receiver. We see that as k increases, the $h^{(k)}(t)$ successively become broader in time, while their integrated areas decrease. Fig. 14(b) compares the simulated impulse response to an experimental measurement, showing that the two are in fairly good agreement. In order to facilitate comparison, the simulated impulse response has been convolved with the impulse response of the experimental measurement system. Simulations of LOS channels are also in good agreement with experimental measurements, leading us to believe that multipath infrared propagation is well described by the model based on multiple diffuse reflections.

As we will see in Section IV, the delay spread of a channel is a remarkably accurate predictor of ISI-induced SNR penalties, independent of the particular time dependence of that channel's impulse response. This suggests that there should exist some functional model for the impulse response having one free parameter, which controls the channel delay spread. By considering an impulse response of this functional form and varying this parameter, one can reproduce a set of channels that produce ISI equivalent in effect to an ensemble of real channels. For purposes of evaluating ISI caused by multipath infrared propagation, this functional model is analogous to the statistical models used in analysis of radio systems. A suitable channel model is obtained by considering a diffuse link consisting of a Lambertian transmitter that is directed toward a diffuse reflector of infinite extent, and a receiver co-located with the transmitter [35]. For such a link, the impulse response can be obtained in closed form as

$$h(t) = H(0) \cdot \frac{6a^6}{(t+a)^7} \cdot u(t) \tag{26}$$

where $u(t)$ is the unit step function and a is related to D, the rms delay spread, by $a = 12\sqrt{11/13} \cdot D$. Although this model is derived by considering an unshadowed diffuse link, it is found to be accurate for LOS and diffuse links, with or without shadowing, as shown in Section IV.

IV. Modulation and Demodulation Techniques

Nondirected infrared channels can be modeled as fixed, linear systems with additive white Gaussian noise (AWGN), as summarized in (1). The transmitted waveform $X(t)$ must be nonnegative, and it is related to the average transmitted optical power P_t by (3). The channel, described by impulse response $h(t)$, exhibits multipath distortion that can cause ISI in high-bit-rate links. When the ISI is relatively mild, it leads to an optical power penalty, but if it is severe, it may lead to a BER floor.

The average transmitted optical power P_t governs the eye safety and electrical power consumption of the transmitter. Hence, the most important criterion for evaluating modulation techniques is the average received optical power P required to achieve a desired BER. We will normalize these received average optical power requirements to those required to achieve the desired BER when transmitting OOK over an ideal channel having impulse response $h(t) = \delta(t)$. That is, on an ideal channel, OOK has a normalized power requirement of 0 dB. We have defined the receiver electrical SNR (5) to be proportional to P^2, so an equivalent criterion is the value of the SNR required to achieve a desired BER. We note that because of this square-law relationship, a 1-dB change in the average power P corresponds to a 2-dB change in the SNR. In evaluating the power or SNR requirements of a modulation technique, at high bit rates one must consider the impact of multipath ISI, as well as any reduction of the ISI that can be achieved through equalization techniques.

It can be difficult to achieve flat frequency response and low noise over a wide bandwidth using large-area photodiodes. Thus the second most important attribute of a modulation technique is the receiver electrical bandwidth

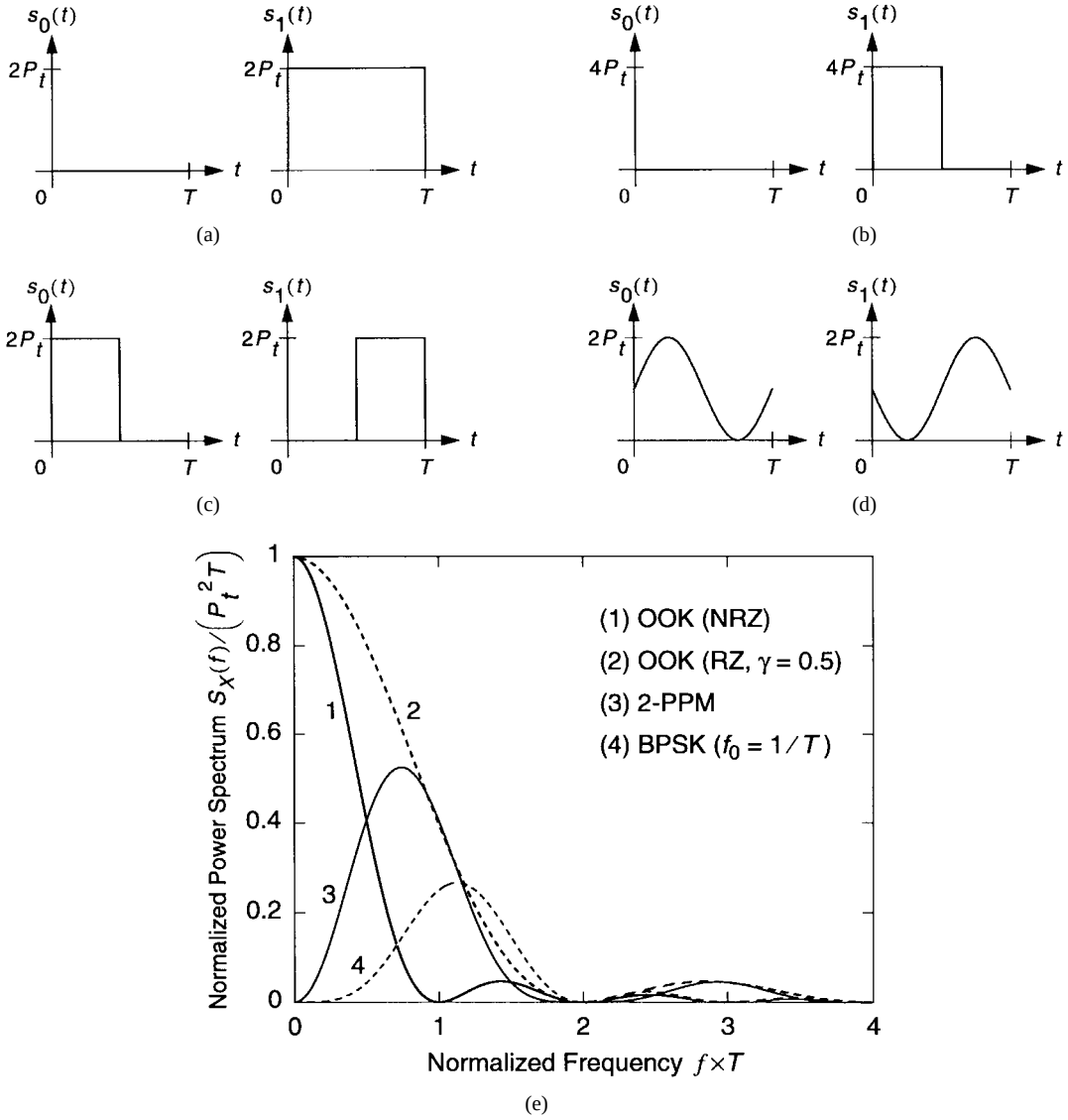

Fig. 15. Common binary modulation schemes. Transmitted waveforms of (a) OOK with NRZ pulse, (b) OOK with RZ pulse of duty cycle $\gamma = 0.5$, (c) 2-PPM, and (d) BPSK subcarrier with subcarrier frequency $f_0 = 1/T$. Corresponding power spectra are shown in (e). In all cases, P_t is the average transmitted optical power and T is the symbol interval (equal to the bit interval).

it requires.[24] For all baseband and single-subcarrier modulation schemes, we define this bandwidth requirement B as the span from dc to the first null in $S_X(f)$, the PSD of the transmitted waveform $X(t)$. For multiple-subcarrier schemes, the bandwidth requirement B is the span from dc to the first null in the highest-frequency subcarrier. We will present bandwidth requirements B/R_b, i.e., normalized to the bit rate R_b. In Fig. 15(a)–(d), we present the waveforms of four common binary modulation techniques: (a) OOK with NRZ pulses, (b) OOK with RZ pulses of duty cycle $\gamma = 0.5$, (c) 2-PPM, and (d) a BPSK subcarrier at a frequency equal to the reciprocal of the symbol duration. A transmission is of the form:

$$X(t) = \sum_{n=-\infty}^{\infty} s_{k_n}(t - nT) \tag{27}$$

where $k_n \in \{0, 1\}$ encodes the nth information bit and $T = 1/R_b$. The PSD's of these four modulations are shown in Fig. 15(e). Based on our definition, OOK with NRZ has a normalized bandwidth requirement of unity, while the other three modulations have twice this normalized bandwidth requirement.

Table 3 and Fig. 16 present a comparison of the power and bandwidth requirements of a number of binary and nonbinary modulation schemes, assuming an ideal channel and AWGN [10], [43]. These modulations include OOK, PPM, differential PPM (DPPM) and multiple-subcarrier

[24] We note that the electrical bandwidth requirement of a modulation technique has little bearing on the optical bandwidth occupied by an IM signal. This optical bandwidth is dominated by the large spectral spread of practical infrared sources. For example, a 1-nm width corresponds to 469 GHz, assuming a wavelength of 800 nm.

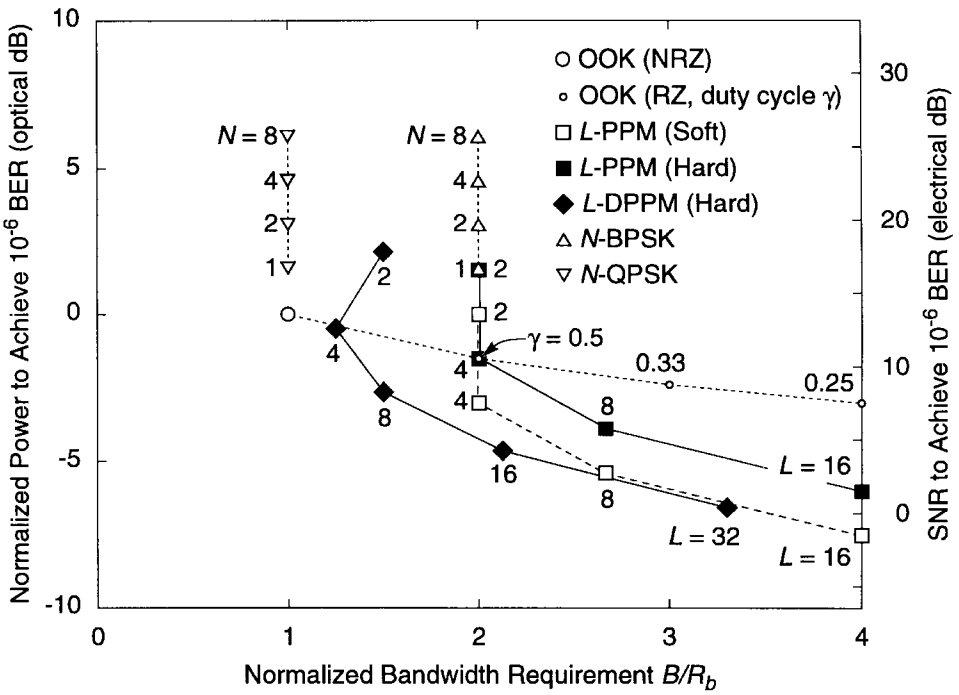

Fig. 16. Theoretical comparison of average power efficiency and bandwidth efficiency of several modulation schemes on nondistorting channels with IM/DD and AWGN. Techniques include OOK with NRZ or RZ pulses, PPM with soft and hard decisions, differential PPM, BPSK subcarriers, and QPSK subcarriers [10], [25], [43].

Table 3 Comparison of Normalized Average Power and Normalized Bandwidth Requirements of Several Modulation Schemes on Ideal Distortionless Channels with AWGN. Some of the Expressions Here Represent Approximations That Are Valid at High SNR. OOK with NRZ Pulses Has Power and Bandwidth Requirements of 0 dB and Unity, Respectively [10], [43]

Modulation Scheme	Normalized Average Power Requirement (Optical dB)	Normalized Bandwidth Requirements
OOK, NRZ	0	1
OOK, RZ, duty cycle γ	$5 \log_{10} \gamma$	$\frac{1}{\gamma}$
N BPSK subcarriers	$1.5 + 5 \log_{10} N$	2
N QPSK subcarriers	$1.5 + 5 \log_{10} N$	1
L-PPM (soft decisions)	$-5 \log_{10}(\frac{L \log_2 L}{2})$	$\frac{L}{\log_2 L}$
L-PPM (hard decisions)	$-5 \log_{10}(\frac{L \log_2 L}{4})$	$\frac{L}{\log_2 L}$
L-DPPM (hard decisions)	$-5 \log_{10}[\frac{L \log_2 L}{8}]$	$\frac{L+1}{2 \log_2 L}$

modulation (MSM) using either binary phase-shift keying (BPSK) or quaternary phase-shift keying (QPSK). In what follows, we discuss the performance of these modulation techniques, including their performance in the presence of multipath ISI and fluorescent-light noise.

A. On–Off Keying

Among all modulation techniques suitable for wireless infrared links, OOK is the simplest to implement. The waveforms of OOK using NRZ pulses and using RZ pulses of duty cycle $\gamma = 0.5$ are shown in Fig. 15(a) and (b), respectively. If the channel is distortionless, the ideal maximum-likelihood (ML) receiver for OOK in AWGN consists of a continuous-time filter matched to the transmitted pulse shape, followed by a sampler and threshold detector set midway between the "low" and "high" pulse amplitudes. Referring to Fig. 16, we see that OOK with NRZ pulses represents a good compromise between the power requirement and bandwidth requirement. The use of RZ pulses having a duty cycle $0 < \gamma < 1$ increases the bandwidth requirement by a factor of $1/\gamma$. However, it decreases the average power requirement, because the increased noise associated with this expanded bandwidth is outweighed by the $1/\gamma$ increase in peak optical power. For this reason, OOK with RZ pulses is utilized in a number of current infrared systems (see Section I-D). However, when the pulse duty cycle is made sufficiently small, we will see that it becomes more efficient to encode information in its position, i.e., to employ PPM.

The performance of OOK on multipath channels without equalization can be computed using the enumeration technique developed in [9]. Fig. 17(a) shows the theoretical power requirements of unequalized OOK (and PPM) links at 10 and 30 Mb/s, computed on an ensemble of about 100 measured multipath channels, which include nondirected-LOS and diffuse configurations, without and with shadowing [17]. We see that the optical power requirement essentially depends only on the *normalized delay spread* (the delay spread normalized to the bit duration), regardless of the link configuration or the particular time dependence of the channel impulse response $h(t)$. On the worst chan-

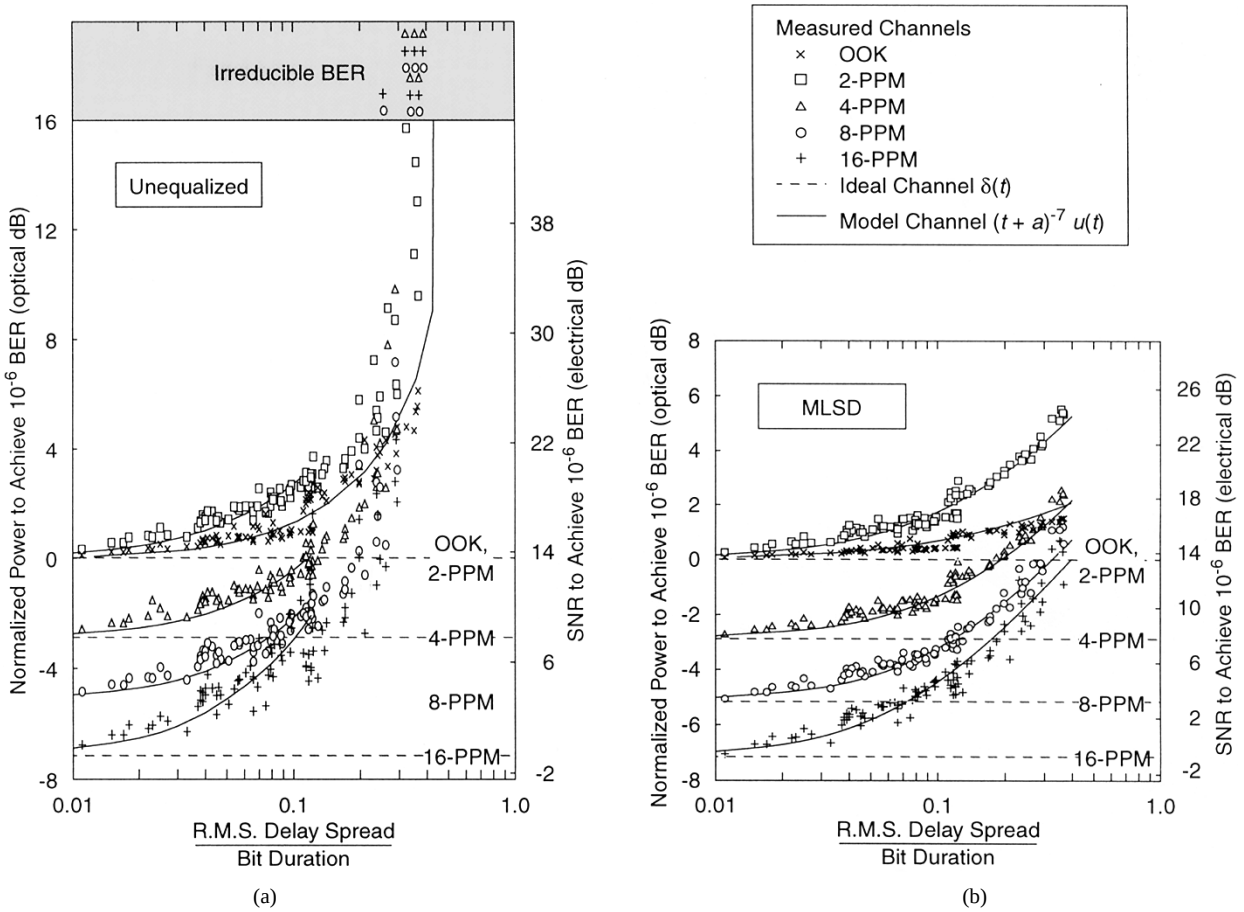

Fig. 17. Theoretical performance of OOK and 2-, 4-, 8-, and 16-PPM at 10 and 30 Mb/s on measured multipath channels using: (a) unequalized receivers, which are optimal only on the ideal channel and (b) optimal MLSD. The dashed lines indicate performance on the ideal channel, and the solid lines indicate performance on model channels having an impulse response of the form $(t + a)^{-7}u(t)$, where a is a parameter governing the delay spread [34], [35].

nels at 30 Mb/s (normalized delay spread of about 0.35), the normalized power requirement is about 6 dB. While relatively high, the power requirement may be acceptable for some applications, particularly when transmitting from a base station. Results for 100 Mb/s are presented in [17], where it is found that unequalized OOK incurs very large power penalties, and develops an irreducible BER for normalized delay spreads above about 0.60, implying that on multipath channels, unequalized OOK reception is not feasible at this bit rate. The solid lines in Fig. 17(a) represent the power requirement computed using the model channel impulse response (26), for different values of the parameter a, which governs the channel delay spread. This model channel reproduces the ISI penalties of real channels remarkably well for all of the modulation/demodulation techniques considered in Fig. 17(a) and (b).

In the presence of multipath ISI, the optimum receiver for OOK employs a whitened matched filter (WMF)[25] front-end and performs maximum-likelihood sequence detection (MLSD), which can be implemented efficiently using the Viterbi algorithm (VA) [45], [47]. Fig. 17(b) shows the theoretical power requirements of 10- and 30-Mb/s OOK (and PPM) links using optimum MLSD, computed on an ensemble of measured channels. We see that with OOK, MLSD is extremely effective in mitigating ISI, reducing the normalized power requirements at 30 Mb/s to less than 2 dB. A practical, though suboptimal, means to mitigate the multipath ISI penalty is by using a decision-feedback equalizer (DFE) [45], [47], which can adapt automatically to the channel impulse response.[26] The power requirements of OOK links using DFE at 10, 30, and 100 Mb/s have been evaluated in [17]. At 10 and 30 Mb/s, power requirements with DFE are very close to those with MLSD, which are shown in Fig. 17(b). At 100 Mb/s, even on the worst channels, no irreducible BER is observed with a DFE, in contrast to the unequalized case, though the normalized power requirements can reach 7.1 dB for shadowed diffuse channels and 9.1 dB for shadowed LOS channels. These power requirements, while high, may be small enough to make OOK with a DFE practical at 100 Mb/s, particularly for transmission from a base station.

[25]The WMF is the optimum front-end for all pulse-amplitude modulation schemes in the presence of ISI and AWGN. It consists of a continuous-time filter matched to the received pulse shape, followed by a sampler and a discrete-time noise-whitening filter [47].

[26]Implementation of the WMF and MLSD require knowledge of the multipath channel impulse response, which is typically learned using an adaptive equalizer, such as a DFE.

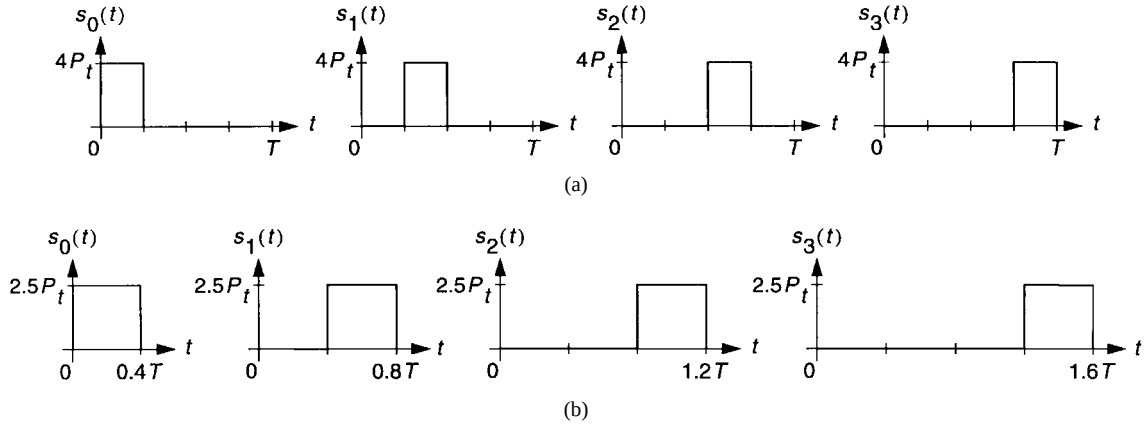

Fig. 18. Comparison of transmitted waveforms for (a) 4-PPM, and (b) 4-differential pulse-position modulation (4-DPPM). P_t is the average transmitted power. In the case of 4-PPM, T represents the symbol duration, while for 4-DPPM, T represents the average symbol duration. In this figure, the two sets of waveforms have been adjusted to correspond to the same peak power and the same average bit rate.

Practical DFE's are implemented using digital or discrete-time analog signal-processing techniques, and usually employ finite-impulse-response filters. As described in Section VII, an experimental 50-Mb/s diffuse link employing OOK with DFE achieved performance close to that predicted by theory [15], [40]. In numerical simulations of a 100-Mb/s OOK link [19], a DFE was found to adapt to a training sequence within about 200 b, i.e., about 2 μs. Most indoor applications of nondirected infrared links will not involve rapidly moving receivers, so that channel impulse responses will change significantly only on time scales of tens to hundreds of ms. Thus we expect that once it is initially adapted to the channel response, a DFE should be able to track easily any changes in that response.

B. Pulse-Position Modulation

PPM is an orthogonal modulation scheme that offers a decrease in average-power requirement compared to OOK, at the expense of an increased bandwidth requirement. L-PPM utilizes *symbols* consisting of L time slots, which we will refer to as *chips*. A constant power LP_t is transmitted during one of these chips and zero power is transmitted during the remaining $L-1$ chips, thereby encoding $\log_2 L$ bits in the position of the "high" chip. Waveforms of 2- and 4-PPM are shown in Fig. 15(c) and Fig. 18(a), respectively. For a given bit rate, L-PPM requires more bandwidth than OOK by a factor $L/\log_2 L$, e.g., 16-PPM requires four times more bandwidth than OOK. In the absence of multipath distortion, L-PPM yields an average-power requirement that decreases steadily with increasing L; the increased noise associated with a $(L/\log_2 L)$-fold wider receiver noise bandwidth is outweighed by the L-fold increase in peak power. This decreased average-power requirement makes PPM especially suitable for portable infrared transmitters. As shown in Section IV-D, PPM can achieve much greater immunity than OOK to near-dc noise from fluorescent lamps. For these reasons, PPM is employed in several commercial wireless infrared systems (see Section I-D). In addition to the increased bandwidth requirement, two drawbacks of PPM, as compared to OOK, are an increased transmitter peak-power requirement, and the need for both chip- and symbol-level synchronization.

In the absence of multipath distortion, an optimum ML receiver for L-PPM employs a continuous-time filter matched to one chip, whose output is sampled at the chip rate. Each block of L samples is passed to a block decoder, which makes a symbol decision, yielding $\log_2 L$ information bits. In *soft-decision decoding*, the samples are unquantized,[27] and the block decoder chooses the largest of the L samples. In *hard-decision decoding*, each sample is quantized to "low" or "high" using a simple threshold detector, and the block decoder makes a symbol decision based on which sample is "high," mediating in cases where no sample, or more than one sample, is "high." While hard decoding is easier to implement, and is thus used in most commercial implementations, it incurs approximately a 1.5-dB optical power penalty with respect to soft decoding [25], [43].[28] Table 3 and Fig. 16 present the power and bandwidth requirements of PPM with soft and hard decoding. For example, 16-PPM has normalized power requirements of -7.5 dB and -6.0 dB with soft and hard decoding, respectively.

When L-PPM is transmitted over multipath channels, the nonzero transmitted chips can induce interference in chips both within the same symbol (intrasymbol interference) and in adjacent transmitted symbols (intersymbol interference); we will refer to these effects collectively as ISI. Fig. 17(a) presents the power requirements of systems employing no equalization [34], i.e., using the same receiver filter and soft-decision decoder that is optimal on a distortionless channel. For small values of the normalized delay spread (i.e., small delay spreads and/or low bit rates), the power requirement is still reduced by employing larger L, and 16-

[27] In a digital implementation of the detector, these samples would be quantized. A resolution of the order of 4–6 b is typically sufficient to achieve near-ideal performance.

[28] This corresponds to a 3-dB SNR penalty, which is fairly typical of binary block codes [45].

PPM yields the best power efficiency among techniques studied. As the normalized delay spread increases, the power requirements increase more rapidly for PPM than for OOK, and increase most rapidly for large L, because of the short chip duration. For the worst channels shown in Fig. 17(a), 4-, 8-, and 16-PPM incur an irreducible BER, unlike OOK and 2-PPM.

When multipath ISI is present, the optimum PPM receiver employs a chip-rate WMF, followed by a MLSD, which can be implemented using a symbol-rate VA [10]. The power requirements of PPM systems using MLSD on multipath channels [34] are shown in Fig. 17(b). The use of MLSD significantly improves the performance of PPM, preventing irreducible BER's and restoring the average-power gain obtained by increasing the value of L. However, as the normalized delay spread increases, even when this optimum detection technique is employed, the power requirements of PPM increase much more rapidly than those of OOK, and on the worst channels, 16-PPM offers only about a 1-dB power advantage over OOK.

There exist several reduced-complexity, suboptimal adaptive equalization techniques for PPM [10], which include linear and DFE's operating at either the chip or symbol rates, as well as hybrid DFE's that make use of tentative chip decisions to cancel intrasymbol interference, but use more reliable symbol decisions to cancel intersymbol interference. At 10 and 30 Mb/s on measured multipath channels, their performance is close to the optimum MLSD [42].

The performance of PPM on multipath channels can be improved [36] by using trellis-coded modulation (TCM) [57], which is designed to maximize the minimum Euclidean distance between allowed signal sequences. A key concept of TCM is the partitioning of the signal set into subsets having unequal minimum Euclidean distances. Since PPM is an orthogonal modulation scheme, on a distortionless channel, the Euclidean distance between any two symbols is the same, and there is no advantage in performing set partitioning. However, multipath distortion causes the Euclidean distances between PPM symbols to become unequal. Partitioning of the 8-PPM symbol set is illustrated in Fig. 19(a), and Fig. 19(b) shows how the minimum Euclidean distances within the subsets[29] depend on normalized channel delay spread. As the delay spread increases, the distances Δ_0 between symbols with adjacent chips falls quite rapidly, whereas the distances, Δ_1 and Δ_2, between symbols with chips separated by two or four chip periods, respectively, decrease less rapidly. As the delay spread increases, trellis codes designed with proper symbol mapping and set partitioning exploit these differences in distance to improve the system performance as compared to that of uncoded PPM. Reference [36] describes a search for optimal rate-2/3 codes for 8-PPM and rate-3/4 codes for 16-PPM. In Fig. 20, the performance of these codes is compared to that of uncoded 16- and 32-PPM.[30] The parameter ν is the constraint length of the code, and the receiver is assumed to employ optimal MSLD on a trellis of combined code and ISI states. We note that as the delay spread increases, trellis-coded PPM exhibits a much more gradual increase in power requirement than uncoded PPM. Trellis-coded 16-PPM is the most power-efficient technique known for use on multipath channels.

Differential PPM (DPPM) [43] is a simple modification of PPM that can achieve improved power and/or bandwidth efficiency in applications where low cost dictates the use of hard-decision detection and multipath ISI is minimal (e.g., at low bit rates or in directed-LOS links). The 4-PPM and 4-DPPM signal sets are compared in Fig. 18(a) and (b), respectively. Each 4-PPM symbol consist of four chips, of which one is "high" and three are "low." The 4-DPPM symbols omit the "low" chips that follow the "high" chip, and hence have unequal durations. Because of this variable symbol duration, symbol boundaries are not known prior to detection, and optimal soft decoding of DPPM requires use of MLSD, even in the absence of coding or ISI. If hard decoding is used, DPPM is easier to decode than PPM, since the former requires no symbol-level timing recovery. The power and bandwidth requirements of DPPM are shown in Fig. 16. Using hard decoding, for a fixed L, DPPM requires much less bandwidth and slightly *more* power than PPM, mainly because the former has a higher duty cycle. If we compare 16-DPPM to 4-PPM, however, we see that 16-DPPM requires 6% more bandwidth, but requires 3.1 dB less optical average power. Because of the variable symbol duration, DPPM offers a nonuniform throughput,[31] which may be problematic for some applications. Reference [43] describes several techniques for mitigating this throughput variation. The performance of DPPM in the presence of multipath ISI is currently under investigation.

C. Subcarrier Modulation

In single-subcarrier modulation (SSM) [10], [33], a bit stream is modulated onto a radio-frequency subcarrier, and this modulated subcarrier is modulated onto $X(t)$, the instantaneous power of the infrared transmitter. Because the subcarrier is typically a sinusoid taking on negative or positive values, a dc bias must be added to it to satisfy the requirement that $X(t)$ be nonnegative. The transmitted waveforms and PSD of a BPSK subcarrier are shown in Fig. 15(d) and (e), respectively, assuming a subcarrier frequency equal to the bit rate. Such a BPSK subcarrier requires twice the bandwidth of an OOK signal, while a QPSK subcarrier requires the same bandwidth as OOK. After optical-to-electrical conversion at the receiver, the subcarrier can be demodulated and detected using a

[29] More precisely, we compute the minimum distance between all possible symbol sequences ending with a symbol drawn from the subset.

[30] Note that rate-2/3 coded 8-PPM has the same bandwidth requirement as uncoded 16-PPM, while rate-3/4-coded 16-PPM requires slightly less bandwidth than uncoded 32-PPM.

[31] To provide an example of nonuniform throughput, assume that the 4-DPPM symbols $s_0(t)$, $s_1(t)$, $s_2(t)$, $s_3(t)$ are used to encode the bit pairs {0, 0}, {0, 1}, {1, 0}, {1, 1}, respectively. Referring to Fig. 18(b), we see that transmission of the bit sequence {0, 0, 0, 0, 0, 0} will require a time 1.2 T, while {1, 1, 1, 1, 1, 1} will require 4.8 T.

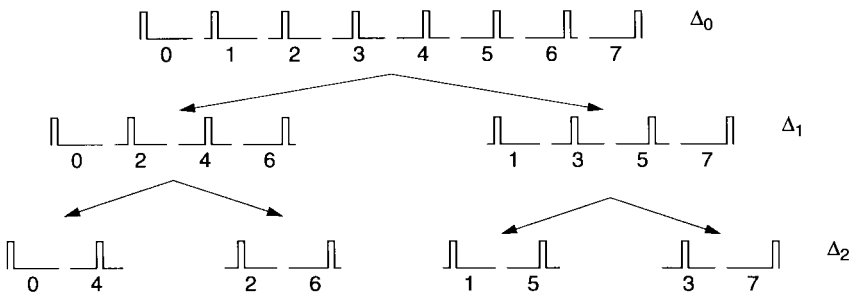

(a)

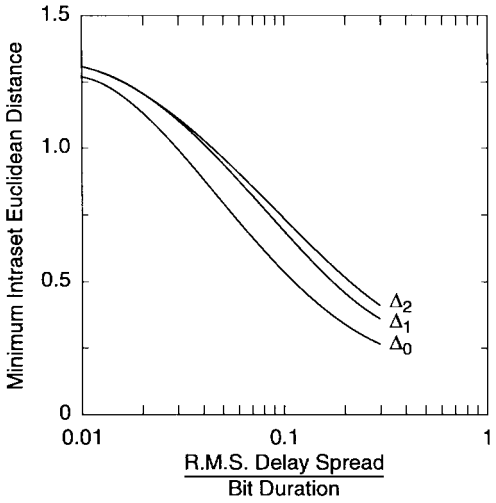

(b)

Fig. 19. (a) Partitioning the 8-PPM signal set. (b) Minimum Euclidean distance between symbols drawn from subsets. In the absence of multipath distortion (zero delay spread), the minimum intraset distances are the same in all three sets. As the channel delay spread increases, the minimum intraset distance decreases most rapidly in the set Δ_0, and least rapidly in the subsets Δ_2 [36].

standard BPSK or QPSK receiver [45]. On distortionless channels, a single BPSK or QPSK subcarrier requires 1.5 dB more optical power than OOK. This can be explained by observing that BPSK and OOK transmissions of average power P_t are equivalent to binary antipodal signals plus a dc bias P_t carrying no information, but the BPSK waveform uses sinusoidal pulses having 3-dB less electrical power, thus requiring 1.5 dB more optical power for achievement of the same receiver SNR.

Multiple-subcarrier modulation (MSM) [10], [33] makes it possible to perform frequency-division multiplexing, while maintaining the simplicity of IM/DD. In MSM, several independent bit streams are modulated onto subcarriers at different frequencies, and their frequency-division-multiplexed sum is used to modulate the intensity of an optical transmitter. At the receiver, the individual bit streams can be recovered using multiple bandpass demodulators. An N-subcarrier transmission requires $5\log_{10}\ N$ dB more optical power than the corresponding single-subcarrier scheme, because the amplitude of each subcarrier must not exceed P_t/N, to insure that $X(t)$ is nonnegative. The power and bandwidth requirements of SSM and MSM systems using BPSK and QPSK on distortionless channels are summarized in Table 3 and Fig. 16.

When MSM is transmitted over a multipath channel, several effects further degrade its power efficiency, as compared to transmission of OOK over an ideal channel [33]. As multipath channels are generally lowpass in nature, subcarriers are subject to an attenuation that generally increases with increasing subcarrier frequency. In addition, subcarriers may be subject to ISI, interference between in-phase and quadrature phases of one subcarrier, and interference between adjacent subcarriers that may overlap partially in frequency. To reduce these three interferences, it is desirable to use a large number of subcarriers, but this leads to an excessive penalty for large N, as described above. We have evaluated the performance of a large number of different MSM schemes, for transmission at total bit rates of 30 and 100 Mb/s over measured multipath channels [33], and have found that the best MSM schemes require several decibels more optical power than OOK with DFE.

While less power-efficient than OOK or L-PPM, MSM may be well suited for transmission of multiplexed bit streams from a base station to a collection of several portable receivers. Through simultaneous transmission of several narrowband subcarriers, MSM can enable very high aggregate bit rates without requiring adaptive equalization to overcome ISI, and may allow individual receivers to

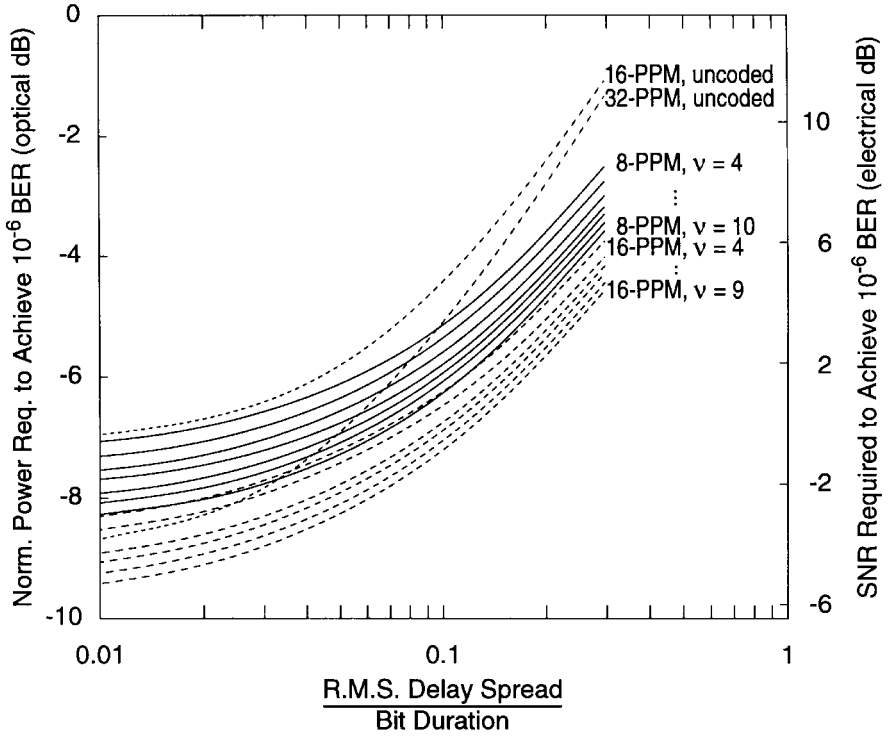

Fig. 20. Theoretical performance of rate-2/3-coded 8-PPM, rate-3/4-coded 16-PPM, and uncoded 16- and 32-PPM. ν represents the constraint length of the code. Receivers employ optimal maximum-likelihood sequence detection on a trellis of combined code and intersymbol-interference states. Multipath distortion is modeled by considering an impulse response of the form $(t+a)^{-7}u(t)$, where a is a parameter governing the delay spread [36].

process only a subset of the total transmission. Furthermore, SSM and MSM can achieve much greater immunity than OOK to near-dc noise from fluorescent lamps, as shown in Section IV-D.

D. Effect of Fluorescent-Light Noise

As mentioned in Section II-D, electronic-ballast fluorescent lamps are potentially much more detrimental to infrared links than their conventional-ballast counterparts. Reference [38] studies the effects of the infrared emission from 22- and 45-kHz electronic-ballast lamps upon various modulation techniques, by computing the BER and optical power requirements in the presence of the nearly periodic fluorescent-light waveform. As an example, Fig. 21 shows the normalized average optical power requirements of 10-Mb/s links in the presence of 22-kHz emissions, as a function of P_f, the optical power received from the fluorescent lamp after optical filtering. This figure considers a single BPSK subcarrier, OOK, and PPM with soft-decision decoding. For the latter two modulation schemes, we consider both receivers employing no highpass filtering and those employing first-order highpass filters that induce sufficient ISI to cause a 2.0-dB SNR penalty, corresponding approximately to the highest cut-on frequency one might employ in the absence of line coding or active baseline restoration.

In principle, subcarrier modulation can be made immune to fluorescent-light noise, by choosing the subcarrier frequency high enough. Hence, a BPSK subcarrier has an optical power requirement that is independent of P_f. When P_f is sufficiently large, OOK suffers a significant penalty from fluorescent-light noise. First-order highpass filtering is not able to reduce the penalty, because the filter cut-on frequency cannot exceed about $0.004R_b$, which is too low to block most of the fluorescent-light noise.[32] For a given value of P_f PPM suffers much smaller penalties than OOK. This can be understood by observing that the OOK slicer is sensitive to the actual values of the fluorescent-light samples, whereas the PPM "choose largest" soft decoder is affected only by the differences among blocks of L samples. For this reason, PPM is less susceptible to fluorescent-light noise at high bit rates, where the block duration is shorter. However, if a PPM receiver employs hard decoding, it loses this "natural" immunity to fluorescent-light noise. We note that simple highpass filtering is effective in countering fluorescent-light noise with PPM, because the continuous component of the L-PPM PSD goes to zero at dc [see, e.g., Fig. 15(e)], so the filter cut-on frequency can be as high as about $0.1R_b$ without inducing excessive ISI.

V. Angle-Diversity Receivers and Quasi-Diffuse Transmitters

An *angle-diversity receiver* utilizes multiple receiving elements that are oriented in different directions. It can be used in place of a single-element receiver in either LOS

[32] As shown in Section VII, the filter cut-on frequency can be raised significantly if active baseline restoration is employed.

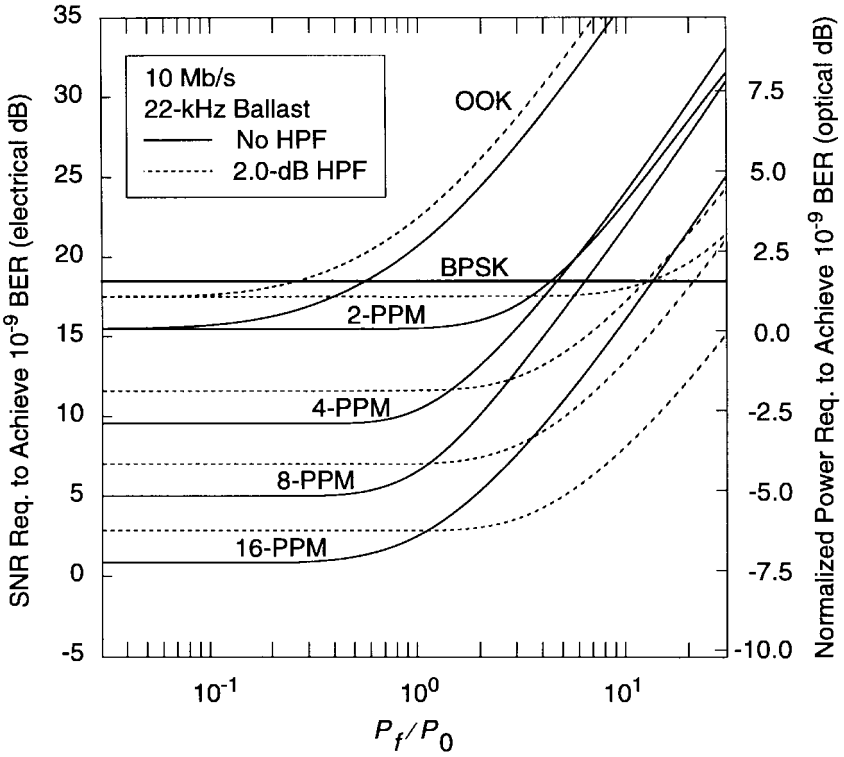

Fig. 21. Theoretical performance comparison of various modulation schemes at 10 Mb/s in the presence of noise from a fluorescent lamp driven by a 22-kHz electronic ballast. Calculations consider two alternate receiver designs: 1) no highpass filter; 2) first-order highpass filter whose cutoff frequency is chosen so that in the absence of fluorescent lighting, the filter induces a 2-dB electrical SNR penalty due to intersymbol interference. The ratio P_f/P_0 represents the maximum absolute excursion (with respect to the mean) of the received fluorescent optical power waveform, divided by the average optical power required to achieve 10^{-9} BER with OOK in the absence of fluorescent lighting [38].

or non-LOS links. In a conventional angle-diversity receiver, each receiving element utilizes its own nonimaging concentrator, such as a CPC or a hemisphere. A CPC-based realization is illustrated in Fig. 22(a), and the angle-dependent effective area of its various elements is shown in Fig. 22(c). A principal advantage of angle-diversity reception is that it allows the receiver to achieve high optical gain and a wide FOV simultaneously, circumventing the gain-FOV trade-off implied in (8). Moreover, an angle-diversity receiver can reduce the impact of ambient light noise, co-channel interference and multipath distortion, in part by exploiting the fact that they are often received from different directions than the desired signal. The advantages achieved by angle-diversity reception depend on how the signals received in the different elements are processed and detected, as summarized in Table 4.

When multipath distortion is significant, the optimum reception technique is *maximum-likelihood combining* (MLC). Assuming that no cochannel interference or fluorescent-light noise is present, a J-element angle-diversity receiver yields J receptions of the form:

$$Y_j(t) = RX(t) \otimes h_j(t) + N_j(t), \qquad j = 1, \cdots, J \quad (28)$$

where $h_j(t)$ is the channel between the transmitter and the jth receiver and the $N_j(t)$ are mutually independent white, Gaussian noises. In MLC, each $Y_j(t)$ is processed by a separate continuous-time matched filter $h_j(-t)$. The J matched-filter outputs are sampled and combined in memoryless fashion, with the jth sample weighted in inverse proportion to the PSD of the noise $N_j(t)$. This weighted sum of the J sample sequences is a sufficient statistic. Using this sufficient statistic, the receiver performs MLSD, which can be implemented using the VA. We note that implementation of MRC requires separate estimation of each of the J channel impulse responses and noise PSD's.

The complexity of MLC is likely to be too high for many applications, and a number of simpler approaches are possible. An easily implemented class of techniques involves combining the $Y_j(t)$ in a memoryless, linear combiner, filtering the weighted sum using a single continuous-time filter, and sampling the filter output. The resulting sample sequence can be processed using MLSD, DFE, or a simple slicer to yield the detected data. This class of techniques includes *maximal-ratio combining* (MRC), *selection diversity* (SD), and *equal-gain combining* (EGC), which differ according to how the combining weights are chosen.

In MRC, the $Y_j(t), j = 1, \cdots, J$, are summed together with weights proportional to the signal current to noise-PSD ratios, thereby maximizing the SNR of the weighted sum. When multipath distortion is not significant, the optimum MLC reduces to MRC followed by a simple slicer.

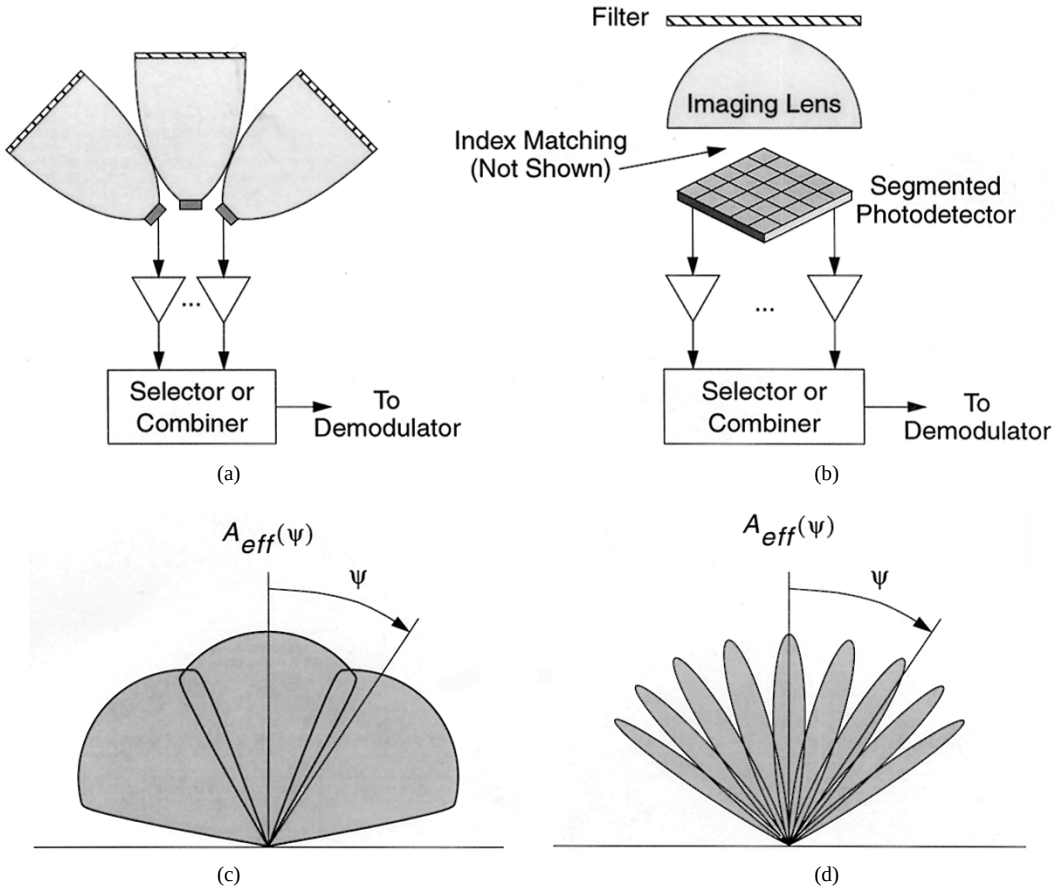

Fig. 22. Angle-diversity receivers using (a) CPC's and (b) an imaging lens and a segmented photodetector. Effective light-collection areas (schematic) of (c) CPC-based receiver and (d) imaging receiver.

Table 4 Combining Techniques for Angle-Diversity Receivers

Advantage	MLC	MRC	Selection Diversity	EGC
Achieves high optical gain and wide field of view simultaneously.	X	X	X	X
Mitigates noise and cochannel interference.	X	X	X	
Mitigates multipath distortion.	X	Under some circumstances.	X	
Can employ a dingle preamplifier				X
Avoids need for channel and noise estimation.				X

Simulations have shown that in diffuse links at low bit rates (where multipath distortion is not a concern), angle-diversity detection with MRC can reduce transmitter optical power requirements by 4–6 dB [28]. MRC can result in a net decrease in multipath distortion, as compared to a single, wide-FOV receiver, as long as both the ambient light noise and multipath reflections both arrive from directions sufficiently far away the strong signal components. If this is not the case, however, an increase in multipath distortion could result. MRC requires estimation of the SNR's in the each of the receiving elements, representing an increase in complexity over nondiversity reception.

In SD, only the signal having the best SNR is utilized. This technique can often separate the signal from ambient-light noise, resulting in a SNR improvement, but the gains are not as large as those achieved using MRC. For example, [14] found that in diffuse links employing angle-diversity receivers, SD requires 1–2 dB more optical power than MRC. SD can yield a significant reduction in multipath distortion, provided that directional receiving elements are employed, making it a promising technique for high-bit-rate systems. Simulations have shown that substantial reductions in multipath delay spread occur when each element has a FOV (semi-angle) smaller than 50° [26]. SD is probably not much simpler to implement than MRC, since it still requires SNR estimation.

In EGC, the multiple signals are summed together with equal weights. This technique increases the receiver FOV, but is unable to separate signal from noise or cochannel interference. Moreover, it can result in an increase of multipath distortion, making it unsuitable for very high-bit-rate links. It is attractive in its simplicity, as it avoids the need for SNR estimation, and the signals from several photodetectors can be processed by a single preamplifier,

provided that the total receiver input capacitance is acceptably small. EGC is used in some diffuse systems at bit rates up to 4 Mb/s, helping them achieve very robust operation, even in the face of shadowing [32].

A promising means to implement angle-diversity reception is by using an *imaging diversity receiver* [8], [31]. This consists of an imaging optical concentrator that has a segmented photodetector array placed at its focal plane, as shown in Fig. 22(b). Each detector output is preamplified separately, and the resulting signals can be processed using either SD, MRC, or MLC.[33] Fig. 22(d) schematically illustrates the angle-dependent effective area of an imaging diversity receiver.[34] An imaging diversity receivers has two major advantages over a nonimaging angle-diversity receiver. First, an imaging receiver employs a planar detector array, which can be monolithically fabricated, enabling the use of a large number of detector segments. Second, the imaging receiver employs one concentrator, regardless of how many detector segments are used. Thus the imaging receiver can use more receiving elements, leading to more effective separation of the signal from unwanted noise and interference. The main disadvantage of the imaging receiver is that it cannot collect light over as wide a FOV as a nonimaging angle-diversity receiver, since the elements of the latter can be oriented in any direction.

The power efficiency of nondirected-non-LOS links can be improved significantly if the diffuse transmitter is replaced by one that emits a number of relatively narrow beams that illuminate a lattice of spots on the ceiling [8], [31]. Each beam should have a divergence angle large enough to make it eye-safe, but small enough that it does not spread excessively when traversing a room. A divergence semiangle of about 2° might be typical. This transmitter design, which we call *quasi-diffuse*, is illustrated in Fig. 23(a). If the signal spots form a regular lattice on the ceiling such that at least one lies within the receiver FOV, then the number of beams required to cover a circle of radius d_h is approximately proportional to d_h^2. The required transmitter power required is proportional to the same factor, i.e., $P_t \propto d_h^2$. Assuming that the beams do not spread much, the propagation loss from the transmitter to the receiver is independent of their horizontal separation d_h, and depends only on the spot-receiver horizontal separation d_{sr}, i.e., $P \propto d_h^0$. Hence the channel gain is proportional to the inverse square of distance, $H(0) \propto d_h^{-2}$, as opposed to the fourth-power dependence characteristic of diffuse links [see (12)].[35]

The quasi-diffuse transmitter design can be combined with either a single-element or angle-diversity receiver to significantly improve the power efficiency of nondirected-non-LOS links. Fig. 23(b) illustrates the transmitter power requirements of 100-Mb/s OOK links [31]. Shot noise induced by ambient light sources is assumed to be the dominant noise source. When a single-element receiver is used, the quasi-diffuse transmitter requires as much as about 10 dB less power than the diffuse transmitter, simply because the former achieves a much higher channel dc gain. If the quasi-diffuse transmitter is employed, exchanging the single-element receiver for a 100-element imaging diversity receiver yields another 10-dB power reduction, because the imaging receiver receives far less ambient light noise than its single-element counterpart.[36] We note that if these links employed PPM instead of OOK, all the transmitter power requirements shown in Fig. 23(b) could be reduced by several dB (see Section IV).

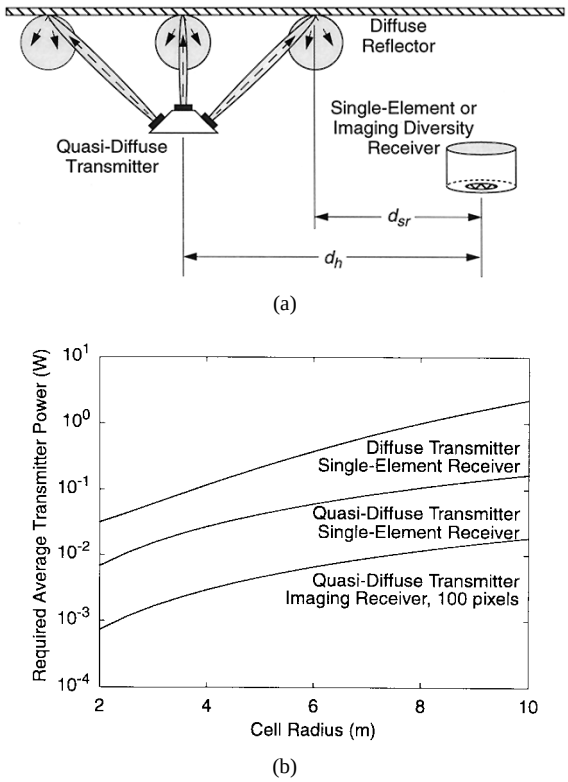

Fig. 23. (a) Nondirected-nonline-of-sight link employing a quasi-diffuse transmitter. (b) Comparison of three nondirected-nonline-of-sight link designs: average transmitter power required to achieve 10^{-9} BER using OOK at 100 Mb/s. Shot noise induced by ambient light is the dominant noise source. In all cases, the transmitter and receiver are located 3 m below the ceiling, which has 100% diffuse reflectivity, and the receiver has a FOV (semiangle) $\Psi_s = 45$, an entrance area $A = 9p/4\ \mathrm{cm}^2$ and a refractive index $n = 1.7$, and it employs a 50-nm-wide optical bandpass filter. The quasi-diffuse transmitter employs a number of beams that ranges between 1 and 11 as the cell radius varies between 2 and 10 m [31].

[33] There is probably no advantage to using an imaging diversity receiver with EGC, because it is unlikely that an imaging concentrator can achieve simultaneously a higher gain and wider overall FOV than a single nonimaging concentrator.

[34] It should be noted that the "dips" in the angle-dependent effective area shown in Fig. 22(d) do not correspond to angles at which the receiver has a significantly smaller overall effective area; rather, they occur when the reception is divided between two or more photodetector segments.

[35] In order to achieve protection against shadowing, it may be desirable that at least two spots lie within the receiver FOV, which would require at least a doubling of the transmitter power P_t.

[36] The power requirements for the 100-element imaging receiver shown in Fig. 23(b) assume that the signal spot falls entirely upon a single photodetector segment, in which case MRC and SD are equivalent. In the worst case, when the spot is incident equally upon three detectors (assuming hexagonal detector segments), and assuming the use of MRC, power requirements for the 100-element imaging receiver are increased from the values shown in Fig. 23(b) by 2.4 dB.

Table 5 Techniques for Multiplexing Transmissions (Shading Denotes an Advantage)

Technique	Nature	Necessary Loss of Per-User Capacity	Optical Average Power Efficiency	Permits Simultaneous Transmission
Wavelength Division	Optical	No	High	Yes
Space Division Multiplexing with Angle Diversity Receiver	Optical	No	High	Yes
Time Division	Electrical	Yes	High	No
Code Division	Electrical	Yes	Moderate	Yes
Subcarrier Frequency Division	Electrical	Yes	Low	Yes

An angle-diversity receiver (of either nonimaging or imaging design) might be used to minimize cochannel interference at a LOS hub, an application that was mentioned in Section I-D. This application is discussed further in Section VI-A, where it is presented as an example of *space-division multiple access*.

VI. Multiple-Access Techniques

In this section, we discuss how multiple users can share the infrared medium, placing emphasis on physical-layer multiplexing techniques, as opposed to medium-access protocols or higher network layers. The medium-access protocols used in some current infrared systems were discussed in Section I-D.

Infrared and radio physical media differ in a number of ways that have significant implications for multiple-access techniques.

1) Infrared cannot pass through walls or other opaque barriers, making it possible to reuse the same infrared bandwidth in each room of a building.
2) As explained in Section I-C, typically it is not practical to perform homodyne or heterodyne detection of the infrared carrier, and DD must be employed. If a DD system employs multiple infrared carriers, these must be separated by optical filtering prior to DD.
3) The short wavelength of infrared makes it possible to achieve high angular resolution in an angle-diversity receiver, e.g., by using imaging optics, as discussed in Section V. This may make it possible to perform space-division multiplexing.
4) Achieving a high SNR is usually the greatest challenge in infrared system design. Achievement of high average-power efficiency with IM favors the use of waveforms having a short duty cycle (see Section IV). This tends to favor the use of time-division multiple access (TDMA) over other electrical multiplexing techniques.
5) The SNR of a DD receiver is proportional to the square of the received optical power [e.g., see (5)]. Because of this, even moderately strong co-channel interference may be "buried" in the thermal and shot noises. It is well known that the capacity of a multiuser system employing bandwidth reuse is maximized when cochannel interference dominates over noise. With infrared systems, however, it is usually not possible to increase the power of all transmitters or decrease the noises until the system becomes interference-limited.

Interference is modeled differently in infrared systems than in radio systems. Consider N simultaneous IM transmissions $X_j(t), j = 1, \cdots, N$, which are incident upon a DD receiver. Let $h_j(t)$ denote the impulse response of the channel between transmitter j and the receiver. Then the total received photocurrent $Y(t)$ is given by

$$Y(t) = R\sum_{j=1}^{N} X_j(t) \otimes h_j(t) + N(t). \tag{29}$$

We emphasize that $Y(t)$ is linear in each of the IM envelopes $X_j(t)$, and that there is no need to consider the relative phases of the underlying optical carriers. The derivation of (29) is a simple generalization of the derivation of (1), which is provided in [17].

We classify techniques for multiplexing transmissions into two categories: optical and electrical. Some of their characteristics are summarized in Table 5.

A. Optical Multiplexing Techniques

Optical multiplexing techniques may permit different users to transmit simultaneously[37] within the same space, without requiring a loss of per-user capacity (at least in principle).

In wavelength-division multiple access (WDMA),[38] different users transmit at different infrared wavelengths using narrow-spectrum sources (e.g., LD's), and a receiver employs a bandpass optical filter to select the desired channel prior to DD. Wavelength-tunable optical transmitters (e.g., tunable LD's) are currently expensive, and fairly sophisticated techniques are required to tune them to a precisely defined wavelength. Large-area, tunable bandpass filters (e.g., single- or multiple-stage Fabry–Perot filters) are costly and, while they could be made in planar form, would be difficult to fabricate in hemispherical form for wide-FOV receivers. Therefore, if a transceiver is to have multiwavelength capability, it must probably include multiple transmitters and receivers, which are likely to be too costly for many applications.

There exist some viable applications of WDMA in which each transceiver needs to transmit at only one wavelength,

[37] That is, using the same time slot, code, or subcarrier frequency.

[38] In order to simplify terminology, multiplexing techniques will include the suffix "multiple access" even when they are not used to provide users with random access to the medium.

and receive at only one wavelength (these two wavelengths may or may not be the same). When used in this manner, WDMA can enable simultaneous, uncoordinated operation of heterogeneous links within the same space. For example, WDMA could enable simultaneous operation of a remote-control device and a data-communication link without interference. As another example, consider a system employing infrared links between portable terminals and a wired backbone network, as shown in Fig. 3(d). WDMA could be used for duplexing the uplinks and downlinks, i.e., all uplinks would employ wavelength λ_1, while all downlinks would use a second wavelength, λ_2. The main drawback of this approach is that it would not permit direct communication between the portables, unless each one were equipped with a second transmitter and/or receiver.

Space-division multiple access (SDMA) involves the use of an angle-diversity receiver (see Section V) to separate signals that are received from different directions. The angle-diversity receiver can be of an imaging or nonimaging design and may employ either SD or MRC. As an example of SDMA, consider a hub capable of establishing simultaneous, independent LOS links with several portable transceivers, as shown in Fig. 3(c). The hub can employ an angle-diversity receiver to minimize co-channel interference between different inbound receptions. In another potential application of SDMA, one might construct a multiple-access LAN using quasi-diffuse transmitters and an imaging angle-diversity receivers, like those shown in Fig. 23(a). Suppose that two quasi-diffuse transmitters are located in close proximity and transmit simultaneously, each illuminating a lattice of spots on the ceiling. If an imaging receiver "sees" a desired signal spot that is not overlapped by a spot from another transmitter, it may be able to detect the desired signal with acceptably small co-channel interference. Assuming that some or all of the transmitters are mobile, as the number of users increases, spot overlap becomes more probable. Hence, this form of SDMA might need to be combined with an electrical multiplexing technique to achieve robust operation.[39]

B. Electrical Multiplexing Techniques

When different users share the same optical channel, electrical multiplexing techniques can enable reliable transmission, but they necessarily entail a loss of per-user capacity (just as in radio systems). The first of these techniques is TDMA, whereby users transmit in nonoverlapping time slots. TDMA has high average-power efficiency, since the transmissions are of low duty cycle, but requires some form of coordination to insure that transmissions do not coincide in time. Since achieving high power efficiency is of paramount importance for portable transmitters, it is not surprising that all current infrared multiple-access LAN's employ some variant of TDMA (see Section I-D).[40] In code-division multiple access (CDMA), different users employ different orthogonal or quasiorthogonal code sequences, permitting them to transmit simultaneously. The power efficiency achieved by CDMA varies, depending upon the duty cycle of the transmitted waveforms. In subcarrier frequency-division multiple access (FDMA), different users can transmit simultaneously at different subcarrier frequencies. The power efficiency achieved by FDMA is poor and worsens as the number of subcarriers increases (see Section IV-C)

We will compare the performance of TDMA, CDMA, and FDMA for infrared within the context of a cellular system with spatial reuse [39]. Specifically, we consider a system that uses diffuse infrared links to access a wired backbone network, like that shown in Fig. 3(d). We will consider the downlinks only, assuming that the uplinks employ a different wavelength or otherwise avoid interfering with the downlinks. Suppose that we wish to provide seamless downlink coverage within a very large room, which requires a very large number of diffuse transmitters. One option is

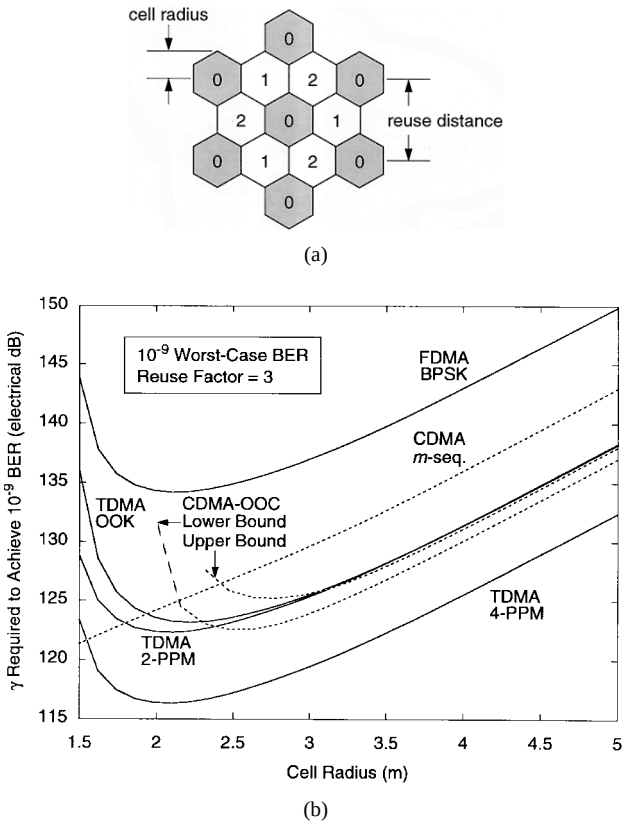

Fig. 24. (a) Fixed assignment of channels in a cellular system having a reuse factor of three. (b) Theoretical performance comparison of six fixed reuse schemes, assuming hexagonal cells and a reuse factor of three. Diffuse transmission is employed, and the throughput in each cell is 10 Mb/s. A BER of 10^{-9} is achieved when the receiver is placed at the worst-case location within the cell (the cell corner). The factor γ is equal to the SNR for unit optical path gain, and is proportional to the square of the transmitted optical power. A 10-dB change in γ corresponds to a 5-dB change in the transmitter optical power [39].

[39] It is interesting to note the analogy between this form of SDMA and CDMA. In this context, the various ceiling-spot arrays can be viewed as quasiorthogonal spatial signals, and an imaging receiver configured to receive one spot array corresponds to a spatial matched filter.

[40] Recall that the SpectrixLite LAN employs CODIAC, a deterministic TDMA protocol, while the IBM diffuse LAN employs CSMA/CA, which can be considered a form of TDMA in which time blocks are randomly utilized by various users.

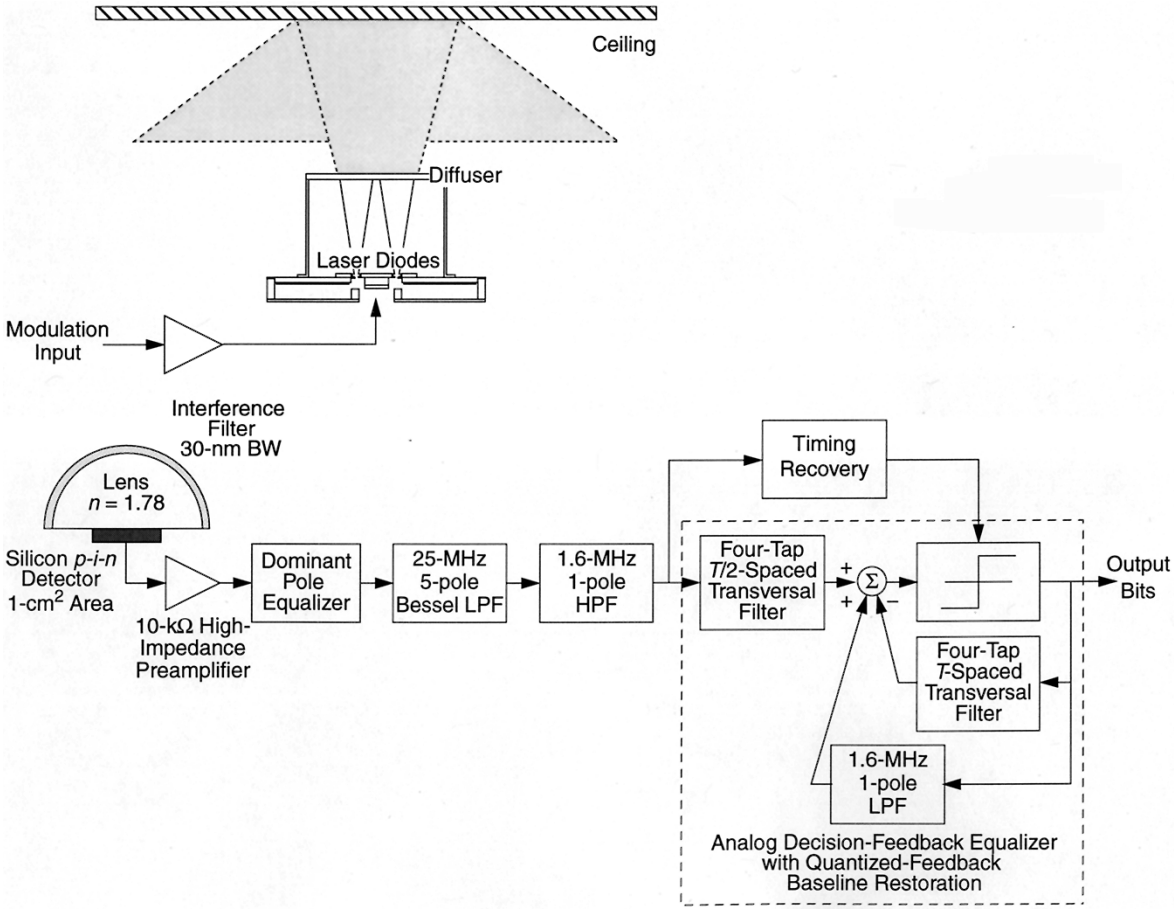

Fig. 25. Design of 50-Mb/s diffuse infrared link employing OOK with DFE [15], [40].

to employ unison broadcast, i.e., to have all transmitters emit identical signals. This technique will lead to increased multipath distortion [10] and requires the entire available bandwidth to be shared by all users within a room.

Here, we consider the use of TDMA, CDMA, or FDMA to divide the downlink bandwidth into several equal partitions; the number of partitions is called the *reuse factor*. The room is divided into cells covered by different downlink transmitters, and equal bandwidth is allocated to each transmitter.[41] The same bandwidth can be reused by nonadjacent transmitters. As an example, Fig. 24(a) shows the layout of a system using a reuse factor of three. Receptions within the central cell numbered "0" are subject to little or no interference from adjacent nearby cells labeled "1" and "2," but are subject to cochannel interference from the six nearby cells labeled "0," which are separated from central cell by the *reuse distance*.[42] The signal-to-cochannel interference ratio (SIR) depends upon the ratio of the reuse distance to the cell radius, and also depends upon how the channel dc gain $H(0)$ varies[43] with the horizontal range d_h. The reuse distance is proportional to the cell radius and to the square root of the reuse factor. In order to increase the SIR, one can either increase the cell radius or increase the reuse factor. As the latter entails a loss of capacity, it is desirable to use the smallest possible reuse factor.

Fig. 24 presents a comparison of the optical average-power efficiency of several fixed cellular reuse schemes [39], including: TDMA with 4-PPM, 2-PPM, and OOK; FDMA with BPSK; and CDMA using m-sequences [45], and optical orthogonal codes (OOC's) [58]. A reuse factor of three is assumed. These calculations consider the gain-versus-range relation of experimentally measured diffuse channels. The throughput in each cell is 10 Mb/s, and a 10^{-9} BER is achieved when the receiver is placed at the worst-case location within the cell (i.e., the cell corner). In order to minimize the transmit power requirement, we wish to minimize the required value of γ, which is equal to the SNR for unit optical path gain, and is proportional to the square of the transmitted optical power. A 10-dB change in γ corresponds to a 5-dB change in the transmitter optical power.

In Fig. 24, we see that for cell radii smaller than 2 to 2.5 m, the required value of γ increases, because of cochannel interference, and at very small cell radii, it becomes impossible to achieve 10^{-9} BER (this does not occur with CDMA using m-sequences, making this the only viable scheme for these small cell radii). Of greater practical

[41] Higher capacity can be achieved by dynamically allocating bandwidth to transmitters depending upon the number of portables each is presently serving, though at the price of increased complexity.

[42] In TDMA and FDMA systems, no interference is received, assuming perfect synchronization and the absence of multipath distortion. In CDMA systems, the adjacent cells "1" and "2" do interfere with cell "0."

[43] Recall that in diffuse links at large d_h, $H(0) \propto d_h^{-4}$ (see Section II-C).

interest, at cell radii larger than about 3 m, where the curves for all modulation schemes become parallel, all modulation schemes become noise-limited, i.e., the performance is virtually the same as if there were no cochannel interference present. In this regime, the lowest power requirement is achieved by TDMA with 4-PPM, the lowest-duty-cycle modulation considered, while FDMA with BPSK has the highest power requirement. The comparison made here does not consider the bandwidth requirement, nor the effect of multipath distortion [39].

VII. Experimental 50-Mb/s Diffuse Infrared Link

We have built and tested an experimental 50-Mb/s diffuse infrared link using OOK [15], [40]. The main goals of this project were 1) to explore the performance limits of very high-bit-rate diffuse infrared links, and 2) to test the performance of a wide-FOV, narrowband receiver based on a hemispherical concentrator and hemispherical bandpass filter. The link design is depicted in Fig. 25. The transmitter uses a cluster of eight LD's whose output is passed through a translucent plastic diffuser to create an approximately Lambertian radiation pattern having 475-mW average power at a wavelength of 806 nm. In typical operation, the transmitter emission is directed upward toward the ceiling, creating a diffuse link configuration. In order to create a receiver having large collection area, wide FOV and narrow passband, a 1-cm^2 silicon p-i-n detector is index-matched to a hemispherical concentrator of 2-cm radius, having a refractive index of 1.78. An optical bandpass filter having a 30-nm bandwidth centered at 815 nm is bonded to the hemisphere's outer surface. This filter-concentrator combination achieves a bandwidth of 30 nm, a net gain $g(\psi)T_s(\psi)$ ranging from 0.5 to 1.75 dB, and a FOV $\Psi_c > 70°$. The photodiode capacitance of 35 pF, in conjunction with the preamplifier load resistance of 10 kΩ, leads to a 455-kHz pole that is compensated by a passive R-C equalizer. The equalized receiver achieves a 3-dB cutoff frequency of 25 MHz, which is limited by the transit time of holes across the depletion region of the photodiode, which is illuminated through the n contact. The preamplifier has an input-referred thermal noise variance of $\sigma^2_{\text{thermal}} = 8.2 \times 10^{-16}$ A^2 when a five-pole, 25-MHz Bessel lowpass receive filter is employed. Residual interference from fluorescent lighting is removed using a 1.6-MHz, single-pole highpass filter, and quantized feedback through a 1.6-MHz, single-pole lowpass filter is used to prevent baseline wander. In order to reduce the impact of multipath ISI, the receiver employs a DFE, with the forward and reverse filters realized using cable delays and manually adjusted, variable-gain amplifiers. Both filters have four taps; those of the forward filter are half-baud-spaced, while those of the reverse filter are baud-spaced.

Fig. 26(a) presents the BER performance of the system in the presence of various ambient lighting conditions. The emission from fluorescent lamps driven by 22-kHz electronic ballasts induces only about a 0.1-dB power penalty, while bright skylight causes a penalty of about

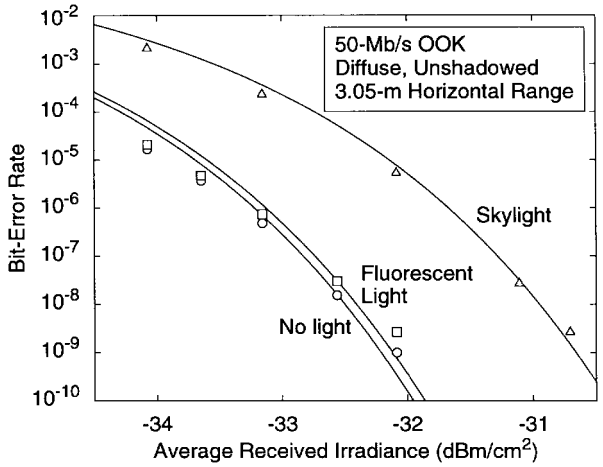

(a)

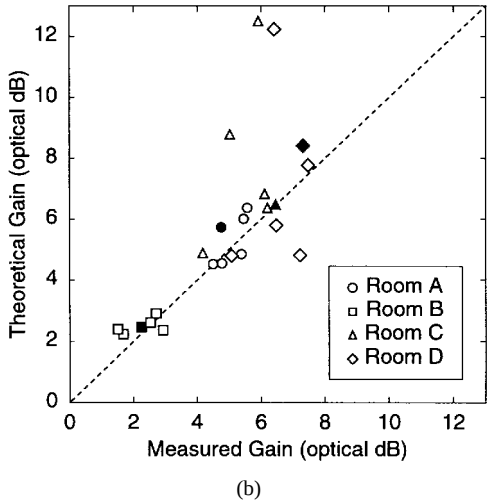

(b)

Fig. 26. Performance of 50-Mb/s diffuse infrared link. (a) BER versus received signal irradiance under various types of ambient lighting. (b) Comparison between theoretical and measured optical power gains achieved by DFE on various multipath channels. Solid symbols denote shadowed link configurations [15], [40].

1.6 dB. The simple DFE is extremely effective in countering multipath ISI, yielding performance gains as high as about 7 dB (optical power), corresponding to a 14-dB SNR gain. Measured performance gains are in excellent agreement with the predictions of theory, which can be seen in Fig. 26(b). In the absence of shadowing and ambient lighting, the link achieves a horizontal transmission range of about 4.4 m (at 10^{-7} BER), while bright skylight reduces this range to about 2.9 m.

VIII. Conclusions

As portable computers and communication terminals become more powerful and are more widely deployed, the demand for high-speed wireless communication is increasing. Infrared represents an attractive choice for many short-range applications. Its advantages include the availability of a wide bandwidth that is unregulated worldwide and that can be reused in a very dense fashion, immunity to

eavesdropping, the ability to achieve very high bit rates, low signal-processing complexity, and potentially very low cost. The most difficult challenge in infrared link design is achieving a high SNR, but major improvements in link efficiency are possible through careful transmitter and receiver design. The unique nature of the IM/DD infrared channels necessitates reexamination of what are appropriate modulation and multiple-access techniques. In most applications, average-power efficiency is of paramount importance, favoring the use of PPM-based modulation schemes and TDMA-based multiple-access techniques. Multipath propagation causes significant ISI in nondirected links at bit rates above 10 Mb/s, but can be mitigated through proper modulation and detection techniques. Advanced components, such as quasi-diffuse transmitters and angle-diversity receivers, promise significant increases in link efficiency and bit rate, at the price of increased complexity.

ACKNOWLEDGMENT

The authors are grateful for the valuable contributions of M. D. Audeh, J. B. Carruthers, H. T. Chee, K. P. Ho, W. J. Krause, C. S. Lee, D. C. Lee, E. A. Lee, G. W. Marsh, D. G. Messerschmitt, R. K. Narasimhan, T. D. Nguyen, D. S. Shiu, and A. P. Tang.

REFERENCES

[1] F. R. Gfeller and U. H. Bapst, "Wireless in-house data communication via diffuse infrared radiation," *Proc. IEEE*, vol. 67, pp. 1474–1486, Nov. 1979.
[2] Y. Nakata, J. Kashio, T. Kojima, and T. Noguchi, "In-house wireless communication system using infrared radiation," *Proc. 7th Int. Conf. on Computer Commun.*, Sydney, Australia, Oct. 30–Nov. 2, 1984, pp. 333–337.
[3] M. D. Kotzin, "Short-range communications using diffusely scattered infrared radiation," Ph.D. dissertation, Northwestern Univ., Evanston, IL, June 1981.
[4] M. E. Marhic, M. D. Kotzin, and A. P. van den Heuvel, "Reflectors and immersion lenses for detectors of diffuse radiation," *J. Optical Soc. Amer.*, vol. 72, no. 3, pp. 352–355, Mar. 1982.
[5] M. D. Kotzin and A. P. van den Heuvel, "A duplex infrared system for in-building communications," in *IEEE Vehic. Technol. Conf. Proc.*, pp. 179–185, 1986.
[6] T. S. Chu and M. J. Gans, "High speed infrared local wireless communication," *IEEE Commun. Mag.*, vol. 25, no. 8, pp. 4–10, Aug. 1987.
[7] A. Lessard and M. Gerla, "Wireless communication in the automated factory environment," *IEEE Network Mag.*, vol. 2, no. 3, pp. 64–69, May 1988.
[8] G. Yun and M. Kavehrad, "Spot diffusing and fly-eye receivers for indoor infrared wireless communications," in *Proc. 1992 IEEE Conf. on Sel. Topics in Wireless Commun.*, Vancouver, B.C., Canada, June 25–26, 1992, pp. 286–292.
[9] J. R. Barry, J. M. Kahn, W. J. Krause, E. A. Lee, and D. G. Messerschmitt, "Simulation of multipath impulse response for wireless optical channels," *IEEE J. Select. Areas in Commun.*, vol. 11, no. 3, pp. 367–379, Apr. 1993.
[10] J. R. Barry, *Wireless Infrared Communications*. Boston: Kluwer, 1994.
[11] F. R. Gfeller, P. Bernasconi, W. Hirt, C. Elisii, and B. Weiss, "Dynamic cell planning for wireless infrared in-house data transmission," in *Mobile Commun.: Advanced Syst. and Components, Proc. 1994 Int. Zurich Seminar on Digital Commun.*, Zurich, Switzerland, Mar. 8–11, 1994, pp. 261–272.
[12] M. J. McCullagh and D. R. Wisely, "155 Mb/s optical wireless link using a bootstrapped silicon APD receiver," *Electron. Lett.*, vol. 30, no. 5, pp. 430–432, 1994.
[13] H. Hashemi, G. Yung, M. Kavehrad, R. Behbahani, and P. A. Galko, "Indoor propagation measurements at infrared frequencies for wireless local area networks applications," *IEEE Trans. Vehic. Technol.*, vol. 43, pp. 562–576, Aug. 1994.
[14] R. T. Valadas and A. M. de Oliveira Duarte, "Sectored receivers for indoor wireless optical communication systems," in *Proc. 5th IEEE Int. Symp. on Personal, Indoor, and Mobile Radio Commun.*, The Hague, The Netherlands, Sept. 21–23, 1994, pp. 1090–1095.
[15] G. W. Marsh and J. M. Kahn, "50-Mb/s diffuse infrared free-space link using on-off keying with decision feedback equalization," *IEEE Photon. Technol. Lett.*, vol. 6, no. 10, pp. 1268–1270, Oct. 1994.
[16] J. P. Savicki and S. P. Morgan, "Hemispherical concentrators and spectral filters for planar sensors in diffuse radiation fields," *Appl. Optics*, vol. 33, no. 34, pp. 8057–8061, Dec. 1994.
[17] J. M. Kahn, W. J. Krause, and J. B. Carruthers, "Experimental characterization of non-directed indoor infrared channels," *IEEE Trans. Commun.*, vol. 43, pp. 1613–1623, Apr. 1995.
[18] K. P. Ho and J. M. Kahn, "Compound parabolic concentrators for narrow-band wireless infrared receivers," *Opt. Engineering*, vol. 34, no. 5, pp. 1385–1395, May 1995.
[19] M. D. Audeh and J. M. Kahn, "Performance evaluation of baseband OOK for wireless indoor infrared LAN's operating at 100 Mb/s", *IEEE Trans. Commun.*, vol. 43, no. 6, pp. 2085–2094, June 1995.
[20] J. R. Barry and J. M. Kahn, "Link design for non-directed wireless infrared communications," *Appl. Optics*, vol. 34, no. 19, pp. 3764–3776, July 1995.
[21] H. Park and J. R. Barry, "Modulation analysis for wireless infrared communications," in *Proc. IEEE Int. Conf. on Commun.*, Seattle, WA, June 18–22, 1995, pp. 1182–1186.
[22] T. D. Nguyen, M.S. report, Univ. Calif., Berkeley, July 1995.
[23] D. B. Medved and R. Halpern, "UWIN: A universal wireless infrared network system," in *Proc. SPIE Conf. on Wireless Commun.*, vol. 2556, San Diego, CA, July 12–13, 1995, pp. 294–304.
[24] D. B. Medved and Y. Azancot, "Wireless optical communication for FDDI, fast Ethernet and ATM connectivity," in *Proc. SPIE Conf. on Wireless Commun.*, vol. 2556, San Diego, CA, July 12–13, 1995, pp. 294–304.
[25] M. D. Audeh, "Power-efficient modulation for high-speed non-directed wireless infrared communication," Ph.D. dissertation, Univ. Calif., Berkeley, 1995.
[26] C. R. A. T. Lomba, R. T. Valadas, and A. M. de Olveira Duarte, "Sectored receivers to combat the multipath dispersion of the indoor optical channel," in *Proc. 6th IEEE Int. Symp. on Personal, Indoor and Mobile Radio Commun.*, Toronto, Canada, Sept. 27–29, 1995, pp. 321–325.
[27] H. Zeino and M. Misson, "Adaptive infrared time-division multiple access (AIR TDMA) for an in-house wireless hybrid LAN," in *Proc. 6th IEEE Int. Symp. on Personal, Indoor, and Mobile Radio Commun.*, pp. 332–337, Toronto, Canada, Sept. 27–29, 1995.
[28] A. M. R. Tavares, R. J. M. T. Valadas, and A. M. de Olveira Duarte, "Performance of an optical sectored receiver for indoor wireless communication systems in presence of artificial and natural noise sources," in *Proc. SPIE Conf. on Wireless Data Transmission*, vol. 2601, Philadelphia, PA, Oct. 23–25, 1995, pp. 264–273.
[29] P. P. Smyth, P. L. Eardley, K. T. Dalton, D. R. Wisely, P. McKee, and D. Wood, "Optical wireless: A prognosis," in *SPIE Proc. on Wireless Data Transmission*, vol. 2601, Philadelphia, PA, Oct. 23–25, 1995, pp. 212–225.
[30] P. Nicholls, R.T. Unwin, and K. T. Dalton, "A 10 Mb/s optical wireless Ethernet: Practical results," in *Proc. SPIE Conf. on Wireless Data Transmission*, vol. 2601, Philadelphia, PA, Oct. 23–25, 1995, pp. 294–304.
[31] A. P. Tang, J. M. Kahn, and K. P. Ho, "Wireless infrared communication links using multi-beam transmitters and imaging receivers," in *Proc. IEEE Int. Conf. on Commun.*, Dallas, TX, June 23–27, 1996, pp. 180–186.
[32] F. Gfeller, W. Hirt, M. de Lange, and B. Weiss, "Wireless infrared transmission: How to reach all office space," in

Proc. IEEE Vehic. Technol. Conf., Atlanta, GA, Apr. 1996, pp. 1535–1539.
[33] J. B. Carruthers and J. M. Kahn, "Multiple-subcarrier modulation for non-directed wireless infrared communication," *IEEE J. Select. Areas in Commun.*, vol. 14, pp. 538–546, Apr. 1996.
[34] M. D. Audeh, J. M. Kahn, and J. R. Barry, "Performance of pulse-position modulation on measured non-directed indoor infrared channels," *IEEE Trans. Commun.*, vol. 44, pp. 654–659, June 1996.
[35] J. B. Carruthers and J. M. Kahn, "Modeling of non-directed wireless infrared channels," *Proc. IEEE Int. Conf. on Commun.*, Dallas, TX, June 23–27, 1996, pp. 1227–1231.
[36] D. C. Lee, J. M. Kahn, and M. D. Audeh, "Trellis-coded pulse-position modulation for indoor wireless infrared communications," in *Proc. 7th IEEE Int. Symp. on Personal, Indoor, and Mobile Radio Commun.*, Taipei, Taiwan, Oct. 15–18, 1996, pp. 349–353.
[37] R. Valadas *et al*., "Experimental results of a pulse-position modulation infrared transceiver," in *Proc. 7th IEEE Int. Symp. on Personal, Indoor, and Mobile Radio Commun.*, Taipei, Taiwan, Oct. 15–18, 1996, pp. 252–256.
[38] R. Narasimhan, M. D. Audeh, and J. M. Kahn, "Effect of electronic-ballast fluorescent lighting on wireless infrared links," *IEE Proc.-Optoelectron.*, Dec. 1996.
[39] G. W. Marsh and J. M. Kahn, "Channel reuse strategies for indoor infrared wireless communications," to be published in *IEEE Trans. Commun.*
[40] ——, "Performance evaluation of experimental 50-Mb/s diffuse infrared wireless link using on-off keying with decision-feedback equalization," *IEEE Trans. Commun.*, vol. 44, pp. 1496–1504, Nov. 1996.
[41] A. J. C. Moreira, R. T. Valadas, and A. M. de Olveira Duarte, "Optical interference produced by artificial light," to be published in *Wireless Networks*.
[42] M. D. Audeh, J. M. Kahn, and J. R. Barry, "Decision-feedback equalization of pulse-position modulation on measured non-directed indoor infrared channels," *IEEE Trans. Commun.*, June 1996.
[43] D. S. Shiu and J. M. Kahn, "Differential pulse-position modulation for power-efficient optical communication," to be published in *IEEE Int. Conf. on Commun.*, Montreal, Quebec, Canada, June 8–12, 1997.
[44] IrDA Standards can be obtained at `http://irda.org`.
[45] J. G. Proakis, *Digital Communications*, 3rd ed. New York: McGraw-Hill, 1995.
[46] R. D. Gitlin, J. F. Hayes, and S. B. Weinstein, *Data Communications Principles*. New York: Plenum, 1992.
[47] E. A. Lee and D. G. Messerschmitt, *Digital Communication*, 2nd ed. Boston: Kluwer, 1994.
[48] J. D. Parsons, *The Mobile Radio Propagation Channel*. New York: Halsted, 1992.
[49] Int. Electrotech. Commission, *CEI/IEC825-1: Safety of Laser Products*, 1993.J. D. Rancourt, *Optical Thin Films*. New York: Macmillan, 1987.
[50] W. T. Welford and R. Winston, *High Collection Nonimaging Optics*. San Diego: Academic, 1989.
[51] X. Ning, R. Winston, and J. O'Gallagher, "Dielectric totally internally reflecting concentrators," *Appl. Optics*, vol. 26, no. 2, pp. 300–305, Jan. 1987.
[52] B. E. A. Saleh and M. C. Teich, *Fundamentals of Photonics*. New York: Wiley, 1991.
[53] B. L. Kasper, "Receiver design," in *Optical Fiber Telecommunications II*, S. E. Miller and I. P. Kaminow, Eds. New York: Academic, 1988, pp. 689–723.
[54] S. D. Personick, "Receiver design for digital fiber optic communications systems, I and II," *Bell Syst. Techn. J.*, vol 52, no. 6, pp 843–886, July–Aug. 1973.
[55] D. L. Rogers, "Integrated optical receivers using MSM detectors," *IEEE J. Lightwave Technol.*, vol. 9, no. 12, pp. 1635–1638, Dec. 1991.
[56] G. Ungerboeck, "Trellis-coded modulation with redundant signal sets—Part I: Introduction," *IEEE Commun. Mag.*, vol. 25, no. 2, pp. 5–11, Feb. 1987.
[57] J. A. Salehi, "Code division multiple access techniques in optical fiber networks—Part I: Fundamental principles," *IEEE Trans. Commun.*, vol. 37, pp. 824–833, Aug. 1989.

Joseph M. Kahn (Member, IEEE) received the A.B., M.A., and Ph.D. degrees in physics from the University of California at Berkeley in 1981, 1983, and 1986, respectively.

From 1987 to 1990 he was a Technical Staff Member of AT&T Bell Laboratories' Lightwave Communications Research Department, Holmdel, NJ. His research focused on multigigabit-per-second coherent optical fiber transmission systems and related device and subsystems technologies. In 1990 he became a Faculty Member at the University of California at Berkeley, where his research interests include infrared and radio wireless communications and optical fiber communications. He is also a Technical Editor of IEEE PERSONAL COMMUNICATIONS MAGAZINE.

Dr. Kahn received the National Science Foundation Presidential Young Investigator Award. He is a member of the IEEE Communications Society and the IEEE Lasers and Electro-Optics Society.

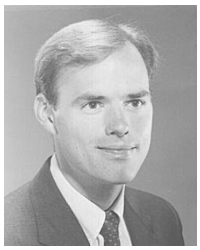

John R. Barry received the B.S. degree from the State University of New York at Buffalo in 1986, and the M.S. and Ph.D. degrees from the University of California at Berkeley in 1987 and 1992, respectively, all in electrical engineering.

Since 1992 he has been an Assistant Professor with the School of Electrical and Computer Engineering at the Georgia Institute of Technology, Atlanta, where his research interests include wireless communications, blind equalization, and multiuser communications. He authored *Wireless Infrared Communications* (Kluwer, 1994).

Dr. Barry received the 1992 David J. Griep Memorial Prize, the 1993 Eliahu Jury Award from University of California at Berkeley, and a 1993 IBM Faculty Development Award.